frontiers in Materials

ORIGINAL RESEARCH
published: 29 January 2019
doi: 10.3389/fmats.2018.00081

Nanostructured Bifunctional Hydrogels as Potential Instructing Platform for Hematopoietic Stem Cell Differentiation

Domenic Kratzer[1,2], *Anita Ludwig-Husemann*[1,2], *Katharina Junges*[1,3], *Udo Geckle*[4] and *Cornelia Lee-Thedieck*[1,2]*

[1] Institute of Functional Interfaces, Karlsruhe Institute of Technology, Eggenstein-Leopoldshafen, Germany, [2] Institute of Cell Biology and Biophysics, Leibniz University Hannover, Hannover, Germany, [3] Faculty 4: Energy-, Process- and Bio-Engineering, University of Stuttgart, Stuttgart, Germany, [4] Institute for Applied Materials – Energy Storage Systems, Karlsruhe Institute of Technology, Eggenstein-Leopoldshafen, Germany

Hematopoietic stem cells (HSCs) are blood forming cells which possess the ability to differentiate into all types of blood cells. T cells are one important cell type HSCs can differentiate into, via corresponding progenitor cells. T cells are part of the adaptive immune system as they mediate cellular immune responses. Due to this crucial function, *in vitro* differentiated T cells are the subject of current studies in the biomedical field in terms of cell transplantation. Studies show that the density of the immobilized Notch ligand Delta-like 1 (DLL1) presented in HSCs' environment can stimulate their differentiation toward T cells. The development of reliable synthetic cell culture systems presenting variable densities of DLL1 is promising for the future expansion of T cells' clinical applications. Here we introduce bifunctional polyethylene glycol-based (PEG-based) hydrogels as a potential instructing platform for the differentiation of human hematopoietic stem and progenitor cells (HSPCs) to T cells. PEG hydrogels bearing the cell adhesion supporting motif RGD (arginyl-glycyl-aspartic acid) were synthesized by UV-light induced radical copolymerization of PEG diacrylate and RGD modified PEG acrylate. The hydrogels were furthermore nanostructured by incorporation of gold nanoparticle arrays that were produced by block copolymer micelle nanolithography (BCML). BCML allows for the decoration of surfaces with gold nanoparticles in a hexagonal manner with well-defined interparticle distances. To determine the impact of DLL1 density on the cell differentiation, hydrogels with particle distances of ∼40 and 90 nm were synthesized and the gold nanoparticles were functionalized with DLL1. After 27 days in culture, HSPCs showed an unphysiological differentiation status and, therefore, the differentiation was evaluated as atypical T lymphoid differentiation. Cluster of differentiation (CD) 4 was the only tested T cell marker which was expressed clearly in all samples. Thus, although the applied nanopatterned hydrogels affected two important signaling pathways (integrins and Notch) for T cell differentiation, it appears that more functionalities that control T cell differentiation in nature need to be considered for achieving fully synthetic *in vitro* T cell differentiation strategies.

Keywords: bifunctional PEGs, nanostructured hydrogels, cell culture, hematopoietic stem cells, T cells

OPEN ACCESS

Edited by:
Hsien-Yeh Chen,
National Taiwan University, Taiwan

Reviewed by:
Jennifer Patterson,
KU Leuven, Belgium
Ahmed El-Fiqi,
Dankook University, South Korea
Jianxun Ding,
Changchun Institute of Applied Chemistry (CAS), China

***Correspondence:**
Cornelia Lee-Thedieck
lee-thedieck@cell.uni-hannover.de

Specialty section:
This article was submitted to Biomaterials, a section of the journal Frontiers in Materials

Received: *26 October 2018*
Accepted: *18 December 2018*
Published: *29 January 2019*

Citation:
Kratzer D, Ludwig-Husemann A, Junges K, Geckle U and Lee-Thedieck C (2019) Nanostructured Bifunctional Hydrogels as Potential Instructing Platform for Hematopoietic Stem Cell Differentiation. Front. Mater. 5:81. doi: 10.3389/fmats.2018.00081

INTRODUCTION

Hematopoietic stem cells (HSCs) are the stem cells of the blood system and provide the human body constantly with fresh blood cells over the course of the entire life cycle. This process of hematopoiesis occurs through the differentiation of HSCs into the individual mature blood cells via the corresponding progenitor cells (Ogawa, 1993). HSCs possess a multipotent potential for hematopoiesis, which means that they can differentiate into any type of blood cells but not into any other cell types (Schütt and Broeker, 2011). T cells are an important type of blood cells which can be formed by differentiation of HSCs. This cell type is an essential part of the adaptive immune system and mediator of cellular immune responses against extraneous structures. T cells are characterized by the presence of an antigen-specific T cell receptor (TCRα/β) expressed at the outer cell surface, which forms a complex with the also presented differentiation marker cluster of differentiation 3 (CD3). Associated with additional differentiation markers CD4 or CD8, the entire complex serves as the cell's "eye," recognizing both extraneous and endogenous antigens and initiating intracellular signal transductions (Murphy et al., 2002; Rink et al., 2015).

The ability to detect and eliminate extraneous structures renders T cells highly interesting for biomedical applications (Moss and Rickinson, 2005). Treatments for diseases of the hematopoietic system (e.g., leukemia) often involve the elimination and replacement of the entire hematopoietic system by means of irradiation or chemotherapy followed by a hematopoietic stem cell transplantation (HSCT). Due to differentiation, migration and maturation processes, T cells need ∼100 days to be formed after the HSCT (Lewin et al., 2002; Bahceci et al., 2003) causing a rather long and risky period of immune deficiency for the patient. But since the T cells differentiate and mature in the recipient's body, they learn to recognize endogenous antigens which circumvent the occurrence of autoimmune reactions (Dumont-Girard et al., 1998; Douek et al., 2000; Roux et al., 2000). An alternative approach provides immediate immune response after HSCT by infusing donor's T cells along with the HSCs (Grob et al., 1987; Boland et al., 1992). The major disadvantage of this approach is the occurrence of the Graft-vs.-Host-Disease (GvHD) in which the donor T cells react against recipient's cells (Shlomchik, 2007; Ferrara et al., 2009; Anasetti et al., 2012). However, a weakened version of this disease in form of the so called Graft-vs.-Tumor (GvT)-effect is absolutely desirable. Here, the transplanted T cells react toward remaining pathological cells that otherwise might initiate a recurrence (Kolb et al., 1990; Carlens et al., 2001; Moss and Rickinson, 2005; Schmid et al., 2006; Welniak et al., 2007; Ferrara et al., 2009). Thus, one is dealing with a tricky balancing act of suppressing the harmful GvHD but maintaining the desired GvT effect after a HSCT. In order to overcome these problems, various studies focus on the effects of the infusion of *in vitro* differentiated progenitor T cells in addition to the HSCs (Donor-Lymphocyte-Infusion). The reconstitution of the cellular immunity proceeds faster in comparison to a T cell-free HSCT, and in addition, the occurrence of GvHD is reduced and simultaneously the GvT-effect is enabled. Furthermore, *in vitro* differentiated T cells are utilized in Donor-Lymphocyte-Infusion to prevent opportunistic infections of patients with eliminated or heavily impaired immune system (Moss and Rickinson, 2005; Park et al., 2006).

The utilization of mature T cells and T cell progenitors in cell-based immunotherapies goes along with the reinforcement of T cell development. Efforts to induce T cell differentiation *in vitro* have been limited mainly due to the fact that the thymus, the organ in which T cells develop, is a complex three-dimensional network of epithelial cells (Holländer et al., 2006). This thymic microenvironment determines T cell lineage commitment via signals critical for T cell generation mediated for instance by Notch ligands Delta-like1 (DLL1) and DLL4, interleukin 7 (IL-7), FMS-like tyrosine kinase 3 ligand (Flt3L), and stem cell factor (SCF) (Pawelec et al., 1998; Besseyrias et al., 2007; Hozumi et al., 2008). Among others, Notch signaling plays an essential role in T cell development. Since it was discovered that HSPCs express Notch receptors (Milner et al., 1994; Varnum-Finney et al., 1998), it was found that Notch1 receptor-mediated signaling is unique in its ability to induce T lineage specification in the thymus while excluding B cell lineage commitment (Radtke et al., 1999; Besseyrias et al., 2007; Hozumi et al., 2008; Koch et al., 2008). There are four Notch receptors (Notch1, 2, 3, and 4) and five structurally related, single-pass transmembrane Notch ligands (DLL1, 3, and 4 and Jagged1 and 2) known so far in mammals (Weber and Calvi, 2010). Notch signaling is based on the direct contact between adjacent cells in which Notch-activating ligands are detected by Notch receptors. In consequence of stimulation by DLL1, the intracellular part of the single-pass transmembrane Notch receptor is first cleaved before migrating to the nucleus where the gene expression is manipulated, which in turn influences proliferation and differentiation behavior.

Immobilized Delta-like1 (DLL1), either cell-bound (Schmitt and Zúñiga-Pflücker, 2002; La Motte-Mohs et al., 2005; Awong et al., 2009; Van Coppernolle et al., 2009) or substrate-bound (Fernandez et al., 2014), specifically induces the Notch signaling cascade (Varnum-Finney et al., 2000). Several studies were published focusing on the application of this concept in cell culture systems. While DLL1 expressing animal feeder cell-based co-culture systems such as OP9-DLL (mouse stromal cells) and FTOC (fetal thymus organ culture) show promising results in terms of Notch ligand-mediated T cell differentiation, the systems lack clinical applicability which requires the use of pure human T cells (Schmitt and Zúñiga-Pflücker, 2002, 2006; Smedt et al., 2004, 2011; Besseyrias et al., 2007; Mohtashami et al., 2010; Van De Walle et al., 2013). Montel-Hagen & colleagues developed an artificial thymic organoid (ATO) system. Therein, DLL1-expressing murine stromal cells are aggregated with human HSPCs to form a 3D-organoid supporting robust differentiation and maturation of human $CD3^+$ $CD8^+$ and $CD3^+$ $CD4^+$ T cells from $CD34^+$ HSPCs (Seet et al., 2017). But the use of murine stromal cells in the ATO system still restricts this application to non-clinical ones. Feeder-free systems involving substrate-immobilized recombinant Notch ligands on synthetic surfaces have also been utilized to induce the differentiation of HSPCs into early T cells (Ikawa et al., 2010; Reimann et al., 2012;

Fernandez et al., 2014). Those systems often require the addition of large amounts of fetal bovine serum and, therefore, suffer from non-robustness due to serum batch-to-batch variations (Gstraunthaler et al., 2013). The addition of animal-based serum furthermore excludes them from clinical applications.

So, the key concept for a Notch-directed stem-cell differentiation into lymphocytes would be a synthetic biomaterial-based system, free of feeder cells and serum. A system recapitulating a minimal thymic niche was developed by Shukla et al. (2017) which is composed of surface-bound DLL4 co-presented with vascular cell adhesion molecule 1 (VCAM-1) in a serum-free medium. The study revealed a threshold concentration of adsorbed DLL4 higher than 7.5 μg/mL to significantly increase the frequency of late stage proT cells after 7 days HSPC culture. Earlier studies on HSPCs revealed a DLL1 concentration dependent proliferation behavior of HSPCs in the context of available cytokines in the *ex vivo* culture. While lower densities of DLL1 in combination with primitive HSPC cytokines promote HSPC expansion on a multi-log scale (Ohishi et al., 2002; Delaney et al., 2005, 2010), higher densities of DLL1 combined with lymphoid cytokines result in T cell lineage commitment and differentiation (Varnum-Finney et al., 2003; Dallas et al., 2005, 2007). Employing a DLL1-functionalized hydrogel system, our group has determined a minimal amount of ∼43,000 DLL1 molecules per cell that is necessary to enhance the proliferation of human umbilical cord blood (UCB)-derived $CD34^+$ HSPCs (Winkler et al., 2017).

To gain ligand-density control of DLL1 presentation to HSPCs and therefore to promote differentiation into T cells, we now present nanostructured bifunctional polyethylene glycol-based (PEG-based) hydrogels as a potential instructing platform for the differentiation of human HSPCs to T cells. Hydrogels are particularly suitable for applications in the field of mammal cell culture due to their structural similarities to the extracellular matrix in terms of water content, soft consistency, and porosity (Nguyen and West, 2002; Drury and Mooney, 2003; Bae et al., 2011). Especially PEG-based hydrogels have been proven to be suitable for cell culture applications (Fairbanks et al., 2009; Aydin et al., 2010; Platzman et al., 2013). PEG-based hydrogels applied in cell culture often require additional functionalization steps in order to interact with the cells. The amino acid sequence arginine-glycine-aspartic acid (RGD) is a cell adhesion motif which is found in many proteins of the extracellular matrix, for example fibronectin (Klein, 1995). Incorporated in PEG-based polymeric networks, the RGD motif has shown to support the adhesion of multiple cell types, such as KG-1a, (Platzman et al., 2013), HSCPs (Muth et al., 2013) and human fibroblasts (Hern and Hubbell, 1998) under maintaining their adhesion potential during cell culture. Two-dimensional nanopatterning by means of block copolymer micelle nanolithography (BCML) provides an elegant way to gain control over the density of immobilized molecules (Altrock et al., 2012; Platzman et al., 2013). On the one hand, loading block copolymer-based micelles can be applied for controlled drug delivery applications (Zheng et al., 2017; Zhang et al., 2018a,b), while on the other hand—in case of BCML—it allows also for the decoration of surfaces with gold nanoparticles (GNPs) in a hexagonal manner with well-defined interparticle distances. The subsequent transfer of the nanoparticles into the hydrogel followed by a further particle functionalization equips the biomaterial with the desired chemical functionality. This concept was already successfully applied in our group to enhance the proliferation of human CB-derived $CD34^+$ HSPCs by presenting immobilized DLL1 in different densities (Winkler et al., 2017). We now expand the application of this promising class of biomaterial and introduce nanostructured, RGD/DLL1 functionalized PEG-based hydrogels as potential instructing platform for the differentiation of human HSPCs to T cells. GNP arrays produced via BCML were transferred to PEG-based hydrogels bearing the cell adhesion supporting motif RGD that were synthesized by free radical polymerization. Subsequently the GNPs were functionalized, resulting in nanostructured hydrogels with immobilized DLL1 in defined densities. To determine the impact of DLL1 density on the cell differentiation of HSPCs, hydrogels with particle distances of ∼40 and 90 nm were applied in cell culture studies.

MATERIALS AND METHODS

Chemicals and Biological Material

Solvents, reagents and chemicals were purchased from Acros, ABCR, Alfa Aesar, Merck, Carl Roth, Sigma-Aldrich, or VWR, unless stated otherwise. All solvents, reagents, and chemicals were used as purchased, unless stated otherwise. Diblock copolymers for BCML were purchased from Polymer Source Inc., Dorval, Canada. DNA dye (Gel Red™) was purchased from Biotum, Hayward, USA. AbC™ capture beads ("positive beads") and "negative beads" were purchased from Invitrogen AG, Carlsbad, USA. Agarose (TopVision™) was ordered from Fermentas GmbH, St. Leon-Rot, Germany. Hepes buffer (99%) was ordered from Amresco LLC, Solon, USA. HPC expansion media, lymphocyte separation media and cytokine mix E were purchased from PromoCell GmbH, Heidelberg, Germany. RGDSK-PEG-acrylate was synthesized and provided by Hubert Kahlbacher, University of Tuebingen, Germany. Medium for T cell differentiation (X-VIVO™10) was purchased from Lonza Group AG, Basel, Switzerland. Loading buffer for gels and buffer for the qualitative PCR were ordered from Peqlab Biotechnologie GmbH, Erlangen, Germany. EDTA-Solution (1% in PBS, without Ca^{2+} and Mg^{2+}) was ordered from Biochrom GmbH, Berlin, Germany. NTA-thiol was given by Max Planck Institute for Intelligent Systems, Stuttgart, Germany. Trypan blue (0.4% for cell culture) was purchased from Amresco, Cleveland, USA. Ultrapure water was in-house manufactured and sterilized using an autoclave. Solvent mixtures are understood as volume/volume. Human $CD34^+$ cells were isolated from donor UCB provided by cord blood banks der Deutschen Knochenmarkspenderdatei, Dresden, Germany, and Deutsches Rotes Kreuz, Mannheim, Germany after prior written, informed consent of the donors and approval by the local ethics committee (B-F-2013-111). CD34-MicroBeads (conjugated with monoclonal murine IgG1-anti CD34-antibody) were purchased from Miltenyi

Biotec, Bergisch-Gladbach, Germany. Bovine serum albumin (Fraktion V, pH 5.2) was purchased from PAA Laboratories GmbH, Pasching, Austria. The following components were purchased from Miltenyi Biotec, Bergisch-Gladbach, Germany: anti-CD3-antibody (human, PE-conjugated), anti-CD4-antibody (human, FITC-conjugated), anti-CD7-antibody (human, PE-conjugated), anti-CD8-antibody (human, PerCP-conjugated), anti-TZRα/β-antibody (human, PE-conjugated), IgG2a-antibody (murine, FITC-, PE- or PerCP-conjugated), IgG2b-antibody (murine, VioBlue-conjugated), Interleukin-2 (IL-2, human, improved sequence), Interleukin-3 (IL-3, human), Interleukin-7 (IL-7, human), Fc-receptor blocking reagent (FcR, human), stem cell factor (SCF, human). Human-delta-like-1 protein (DLL1, human, six-fold histidine tag at the carboxy terminus, produced in the cell line NS0) was purchased from R&D Systems, Minneapolis, USA. Fetal bovine serum (FBS, filtered sterile) was purchased from Sigma Aldrich GmbH, München, Germany. The following components were purchased from Invitrogen AG, Carlsbad, USA: IgG1-antibody (murine, FITC-, PE-conjugated); anti-CD34-antibody (human, PE-conjugated). Anti-CD19-antibody (human, PE-conjugated) and anti-CD2-antibody (human, FITC conjugated) were purchased from ImmunoTools GmbH, Friesoythe, Germany.

Characterization and Technical Devices

Cells were analyzed by flow cytometry using Attune® Acoustic Focusing Cytometer with Attune® Cytometric Software v2.1 by Thermo Fisher Scientific Inc., Waltham, USA. The analysis software FlowJo_V10 was purchased from FlowJo, Ashland, USA. Solid substrates were cleaned and activated in oxygen plasma or hydrogen plasma using a Pico PCCE device by Diener electronic GmbH and Co. KG, Ebhausen, Germany. Nanostructured BCML glass substrates were analyzed by scanning electron microscopy (SEM) using Merlin by Carl Zeiss SMT GmbH, Oberkochen, Germany. The glass samples were first sputtered with a carbon layer of ∼15 nm thickness. The SEM images were captured on three different locations on each surface with 50,000-fold magnification using a backscattered electrons (BSE) detector. The transfer of the GNPs from the glass substrates into the hydrogel as well as the $CD34^+$ cells on hydrogels were also visualized using SEM. SEM images were analyzed using ImageJ 1.50i by Wayne Rasband, National Institutes of Health, Bethesda, USA and the ImageJ plugin dot analyse2. The plugin dot analyse2 was developed by Max Planck Institute for Intelligent Systems, in Stuttgart for the analysis of structures formed by nanoparticles on surfaces. This plugin measures the interparticle distance between each gold nanoparticle and the surrounding nanoparticles, followed by a calculation of the average particle distance as well as the deviation. Additionally, the plugin is able to verify and evaluate the quality of hexagonal arrays based on a mathematical algorithm described by Williges et al. (2013).

$$\Psi_6 = \left| \frac{1}{N_{bonds}} \sum_j \sum_k e^{i6\theta_{jk}} \right| \quad (1)$$

Equation 1. Equation according to Williges et al.

Ψ_6 is called the 6-fold orientational order parameter and its value evaluate the accuracy of the hexagonal structure formed by GNPs. θ is the angle between a central nanoparticle and its two nearest neighboring nanoparticles. $1/N_{bonds}$ normalized the calculated value of Ψ_6. Samples were freeze-dried using a Christ Alpha 1-4 by B. Braun Biotech International, Melsungen, Germany. MACS®-Mixer (MACSmix™ tube rotator) by Miltenyi Biotec, Bergisch-Gladbach, Germany was used for HSC isolation. Ultrapure water (Typ 1 according to the American Society for Testing and Materials) was obtained from Arium® pro System by Sartorius AG, Göttingen, Germany. Spin-coated samples were coated using a WS-650MZ-23NPP by Laurell Technologies Corporation, North Wales, USA. Reactions and solutions were stirred using a Variomag®Poly Komet magnetic stirrer by Thermo Fisher Scientific Inc., Waltham, USA. Small amounts of water-based mixtures were transferred using Eppendorf Research Plus pipettes by Eppendorf, Hamburg, Germany. Solid substances were weighed out using a SI-234 balance by Denver Instruments, Sartorius Corporation, Bohemia, USA. Light-sensitive reactions were conducted using a Vilber Lourmat VL8.L, 8 Watt and 365 nm UV lamp by Vilber, Maren La Vallee, France. Samples which needed ultrasonic treatment were processed in Ultrasonic Cleaner by VWR International GmbH, Radnor, USA. Some samples were centrifuged using a Hereaus Multifuge X3R by Thermo Fisher Scientific Inc., Waltham, USA and Centrifuge 5415 D, 5415 R, or 5418 R by Eppendorf, Hamburg, Germany, respectively. All work with mammalian cells was performed on a sterile bench with laminar air flow. The cells were only in contact with sterile materials. The cultivation took place in sterile cell culture flasks or sterile cell culture plates in incubators at 37°C, 5% CO_2 and 95% humidity.

Methods

Block Copolymer Micellar Nanolithography (BCML)

BCML was used to generate PEG-based hydrogels with hexagonally ordered arrays of GNPs in which the nanoparticles are equally spaced over the entire surface area. The overall process involved several steps including the deposition of inverse diblock copolymer micelles, which were loaded with a gold precursor salt, on glass substrates and the subsequent transfer of the reduced GNPs into the hydrogel (Spatz et al., 2000; Lohmuller et al., 2011).

Initially, several glass substrates bearing nanostructured GNPs with different interparticle distances were produced. For this purpose, diblock copolymer solutions with a concentration of 5 mg/mL in *ortho*-xylene were prepared. For nanoarrays with an average interparticle distance of 40 nm, a block copolymer consisting of 288 styrene subunits and 119 2-vinyl pyridine subunits (PS_{288}-*b*-$P2VP_{119}$, $Đ^* = 1.06$) was employed. Nanoarrays with an average particle distance of 90 nm were produced by applying a block copolymer consisting of 1,056 styrene subunits and 671 2-vinyl pyridine subunits (PS_{1056}-*b*-$P2VP_{671}$, $Đ^* = 1.09$). The polymer solutions were stirred overnight at 300 rpm in order to provide sufficient time for the inverse micelles to be formed. After 24 h, the precursor tetrachloro-auric(III)acid trihydrate ($HAuCl_4 \cdot 3\ H_2O$) was added to the polymer solutions to start the micellar loading

process. In the presented study, the target loading factor L of the polymer micelles was 0.3, which is defined as the amount of precursor salt compared to the amount of 2VP repeating units [$L = n(HAuCl_4 \cdot 3\ H_2O)/n(RU_{2VP})$]. The loading factor defines the particle size of the GNPs on the final glass substrate. The calculation of the corresponding amount of precursor salt was performed according to **Equation 2**.

$$m\ (HAuCl_4 \bullet 3H_2O) = \frac{m\,(polymer) \times M\,(HAuCl_4 \bullet 3H_2O) \times repeating\ units\ 2VP \times loading\ factor}{M\ (polymer)} \quad (2)$$

Equation 2. Calculation of the amount of precursor salt used in BCML.

The gold precursor salt was weighed out using a glass spatula to avoid the undesired reduction of the Au(III) species. After adding the gold salt, the mixture was stirred for additional 24 h at 300 rpm in the dark. Thereafter, the solution was filtered through a polytetrafluoroethylene syringe filter with a pore size of 0.2 μm. Square-shaped glass slides with a size of 18 mm x 18 mm were used as substrates in the BCML process. These were initially cleaned and activated by putting them in Caro's acid (1 part H_2O_2 and 3 parts H_2SO_4) for 1 h. Afterwards, the glass slides were washed with ultrapure water in an ultrasonic bath and dried in a nitrogen flow. In the next step, the activated glass slides were spin coated with the polymer micelle solution. The spin coating process was conducted in a static mode for 1 min with 2,500 rpm for PS_{1056}-*b*-$P2VP_{671}$ and 7,000 rpm for PS_{288}-*b*-$P2VP_{119}$, respectively. After reaching the desired rotation speed, 25 to 50 μL of the corresponding polymer solution was dropped onto the rotating sample from a distance of 3 cm. The interaction between the activated glass surface and the polar micelle cores leads to a self-assembled monolayer of micelles in a quasihexagonal array. In the final step, hydrogen plasma was used to simultaneously remove the organic copolymer micelles and reduce the gold precursor salt to elemental GNPs. For this purpose, the spin coated samples were placed in the plasma chamber for 45 min at 0.4 mbar and 100% performance which corresponds to ∼200 W with the used plasma device.

Synthesis of Hydrogels

PEG700-DA and ultrapure water were mixed in equal parts. The polymerization at a mixing ratio of 1:1 resulted in hydrogels with a swelling ratio of approximately 1 and, therefore, no further swelling occurred in the final hydrogel and the distortion of the nanostructure could be prevented (Aydin et al., 2010). The photoinitiator Irgacure 2959 was dissolved in 70% ethanol so that the concentration was 100 mg/mL. Then, the Irgacure 2959 solution was added to the polymer solution to achieve a concentration of 0.5 mg Irgacure 2959 per mL PEG700-DA. To this mixture, RGDSK-PEG-acrylate was added to achieve a concentration of 32 μM. The crosslinkable polymer solution of PEG700-DA, Irgacure 2959 and RGDSK-PEG-acrylate was centrifuged with 100 rcf for 6 min. The molds for the hydrogel formation were constructed from microscope slides (**Figure 1B**). Initially, a glass cover slip of the size 18 mm x 18 mm was fixated in the middle of the microscope slide. A glass cover slip of the size 24 mm x 60 mm was subsequently placed across two 500 μm high spacers to bridge the central section. Then, 100 μL of the polymer solution was pipetted into the gap between the central cover slip and the overlying cover slip. This way, thicknesses of the resulting hydrogels ranged from 0.34 to 0.37 mm. The polymerization was conducted at 14.8 mW/cm² UVA irradiation with a wavelength of 365 nm for 12 min. The resulting PEG hydrogels were washed three times with ultrapure water at 4°C for at least 2 h in order to remove potentially remaining non-polymerized monomer which acts toxic toward mammalian cells. Finally, the gels could be stored in ultrapure water at 4°C over the course of several months if necessary.

Synthesis of Nanostructured Hydrogels

A 1 mM solution of *N*,*N*'-bis(acryloyl)cystamine (BAC) in ethanol was prepared and placed in an incubator shaker at 400 rpm and 21°C overnight in the dark. The nanostructured glass surfaces were then incubated in the BAC solution for 1 h in the dark in order to form thiol-gold bonds. Following that, the surfaces were washed three times with ethanol for 10 min, dried in nitrogen stream and used immediately for a hydrogel synthesis as described in chapter Synthesis of Nanostructured Hydrogels. The transfer of the nanoparticles was accomplished by replacing the 18 × 18 mm glass slide in the mold used for the regular hydrogel synthesis (chapter Synthesis of Nanostructured Hydrogels) with the corresponding glass substrate bearing BAC-functionalized GNPs. This approach resulted in hydrogels equipped with both the cell adhesion motif RGD and the surface-bound quasi-hexagonally arranged GNPs.

Qualitative Verification of the Transfer of GNPs

An aqueous solution (ultrapure water) of 0.1% $HAuCl_4$ in 0.2 mM hydroxylamine was prepared. The solution was then brought into contact with the nanostructured side of the hydrogel for 5 min. In this process hydroxylamine acts as reducing agent for the dissolved gold cations. The resulting elemental gold is favored to deposit onto the GNPs. After a sufficient growth period, the gold particles could be observed by the appearance of a violet coloration typical for gold colloids appearance (Everett, 1992).

Biofunctionalization of Hydrogels With DLL1

Hydrogels were punched out using a wad punch with a diameter of 15 mm. All following steps were conducted under sterile conditions: The gels were sterilized for 30 min in 70% ethanol. Afterwards, they were briefly dipped three times in 100% ethanol in order to remove water residues for the subsequent reaction step. Afterwards, the samples were put in a petri dish which was placed in a humid chamber. Right after, 50 μL of a 1 mg/mL NTA-thiol solution in ethanol was pipetted onto the hydrogels. A piece of plastic foil which was sterilized with ethanol was affixed bubble-free across the hydrogels to ensure uniform distribution of the solution and as protection against evaporation

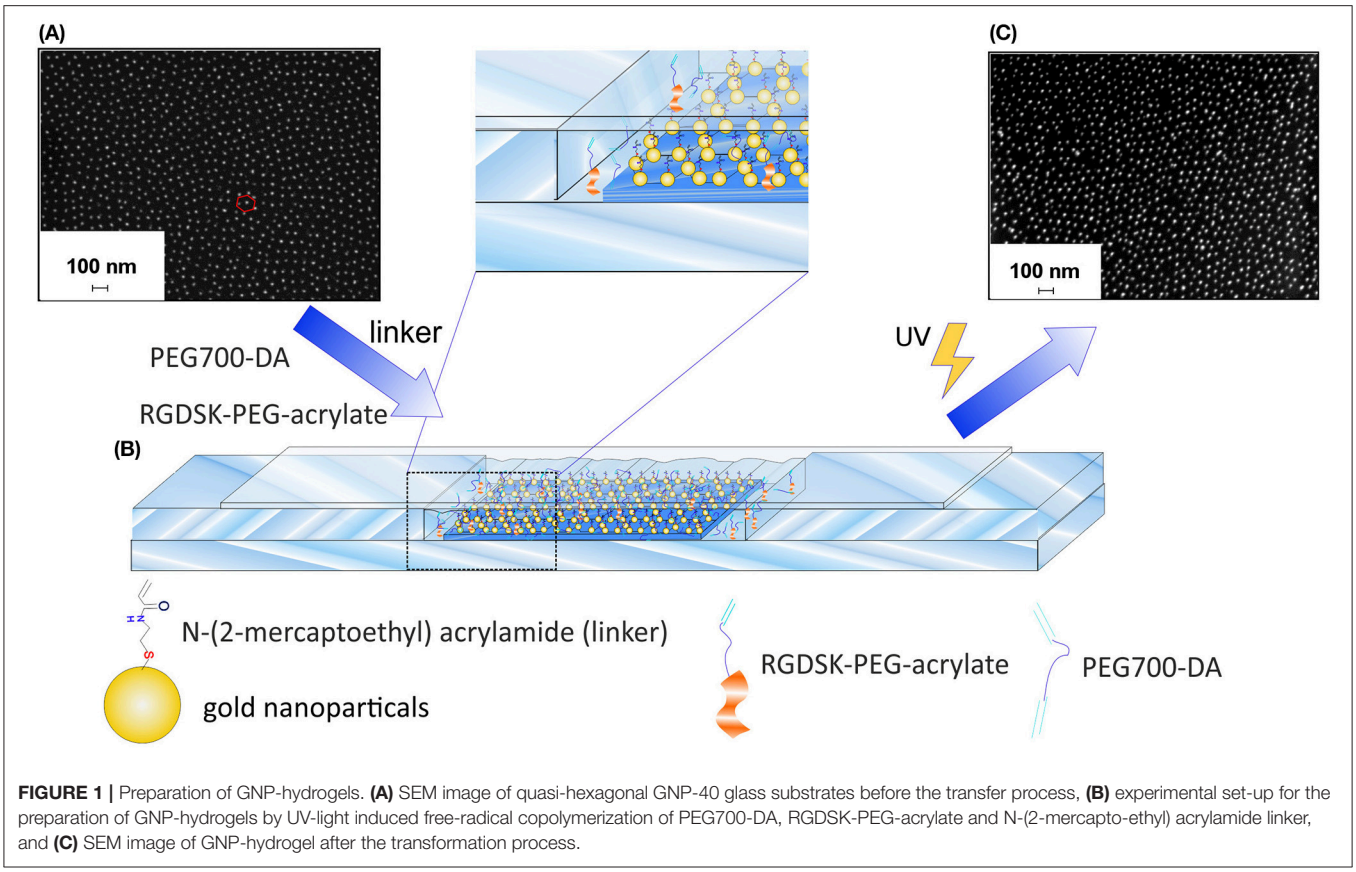

FIGURE 1 | Preparation of GNP-hydrogels. **(A)** SEM image of quasi-hexagonal GNP-40 glass substrates before the transfer process, **(B)** experimental set-up for the preparation of GNP-hydrogels by UV-light induced free-radical copolymerization of PEG700-DA, RGDSK-PEG-acrylate and N-(2-mercapto-ethyl) acrylamide linker, and **(C)** SEM image of GNP-hydrogel after the transformation process.

of ethanol. The humid chamber was closed off airtight and the hydrogels were incubated with in NTA-thiol solution for 1 h in the dark. Following this, the gels were briefly swiveled in 100% ethanol and then washed with 4-(2-hydroxyethyl)-1-piperazineethanesulfonic acid (HEPES)-buffered saline (HBS solution: ultrapure water + 20 mmol/L HEPES + 150 mmol/L sodium chloride, pH adjusted to 7.4 and autoclaved) for ∼2 min. Subsequently the hydrogels were transferred into fresh petri dishes to be incubated in 1 mL of 25 μM nickel chloride solution (HBS solution + 0.1% $NiCl_2$ stem solution; $NiCl_2$ stem solution = HBS solution + 25 mmol/L $NiCl_2$ stem solution) for 15 min in the dark. The nickel solution was then removed by washing with HBS another 2 min. The hydrogel was then placed in phosphate-buffered saline (PBS) for 15 min in the dark. Eventually the hydrogel was transferred into a new petri dish in a humid chamber and evenly covered with 50 μL of a 5 μg/mL DLL1 solution in PBS by affixing a sterilized piece of foil across bubble-free. The humid chamber was closed off airtight and the hydrogel was incubated in the DLL1 solution at 4°C overnight in the dark. After incubation, the cover foil was removed by the addition of PBS. The hydrogels were placed in a cell culture 24-well plate (diameter 15.6 mm) with the biofunctionalized side pointing upwards. The hydrogels were washed twice with PBS and then incubated in 1 mL cell specific medium in an incubator. Thereafter, cells could be seeded onto the hydrogels.

Homogenous gold surfaces were also functionalized with DLL1 in order to obtain control samples for the cell culture experiments. The functionalization of the gold surfaces was done analogously to the above described functionalization of the hydrogels. The resulting gold surfaces were furthermore coated with fibronectin after incubation with DLL1 in order to introduce the RGD motif: gold surfaces were washed twice with PBS and put in a petri dish which was placed in a humid chamber. Fifty microliter of a 5 μg/mL fibronectin solution in PBS were pipetted onto the surfaces and evenly distributed by affixing a sterilized piece of foil across bubble-free. The humid chamber was closed off airtight and the surfaces were incubated for 2 h in the dark. Following this, the gold samples were treated the same way as the biofunctionalized hydrogels after DLL1 incubation.

Preparation of Hydrogels With Semi-adherent Cells for Scanning Electron Microscopy

$CD34^+$ cells were incubated in expansion medium (HPC expansion medium + 1% cytokine mix E + 1% penicillin/streptomycin) overnight on a nanostructured hydrogel with an average interparticle distance of ∼40 nm. The cells were then fixated on the hydrogel in 2.5% glutaraldehyde solution for 2 h. The sample was then dewatered by suspending it in 50, 70, 90, 95, and 100% ethanol for 10 min each. Following this, the hydrogel was stored at −80°C in 100% ethanol overnight, then lyophilized and eventually stored in a desiccator until SEM analysis was conducted. In the current study, the adherent cells on GNP-40 samples were imaged representatively. Cells seeded on DLL1-functionalized GNP-90 hydrogels with equal

concentrations of RGD peptides copolymerized into the PEGDA hydrogels exhibit an equivalent adhesive behavior as shown in a previous study (Winkler et al., 2017).

Isolation of CD 34$^+$ Cells From Human Umbilical Cord Blood

$CD34^+$ cells were isolated from human UCB according to manufacturer's instructions (CD34 MicroBead Kit, human, Miltenyi Biotec, Bergisch Gladbach, Germany). The UCB was processed within 48 h after collection. Purity of $CD34^+$ cells was checked by flow cytometry and was always >99% for cell culture.

Flow Cytometry

The isolated as well as cultivated cells were analyzed by flow cytometry. The expression of markers was examined with the specific antibodies against CD34 for HSPCs, against CD2 and CD7 for early T cells, against CD3, CD4, CD8, and TZRα/β for late T cells, and against CD19 for B cells. For this, 2×10^4 to 1×10^5 cells in 50 μL PBS with 0.1% FBS and 21% FcR blocking reagent were stained with 2.5 μL antibody solution or the respective isotype control at 4°C in the dark for up to 1 h. Following this, the cells were fixed with 3.7% formaldehyde and stored at 4°C in the dark until they were analyzed. Additional information regarding the various marker molecules are listed in the supporting information (**Supplementary Table 1**). Mononuclear blood cells from UCB were used as positive control samples for the flow cytometric antibodies. Those were present in the elution volume after magnetic separation during the $CD34^+$ cell isolation.

T Cell Differentiation of Cluster of Differentiation 34$^+$ Cells on DLL1-Functionalized Nanostructured Hydrogels

The serum-free medium (X-VIVO^{TM} 10) was supplemented with 10 ng/mL FMS-like tyrosine kinase (Flt)3-ligand, 300 ng/mL interleukin (IL)-2, 100 ng/mL IL-3 and 1 ng/mL stem cell factor (SCF), and 100 ng/mL IL-7. Hereafter, this medium will be denoted as T cell differentiation (TCD) medium. Cells were grown in TCD medium and 1% penicillin/streptomycin. The exact function of the various cytokines is described in the supporting information (**Supplementary Table 2**). $CD34^+$ cells, isolated from UCB, were seeded on DLL1 nanostructured hydrogels with a cell number of 2×10^4 cells per surface. In initial experiments $CD34^+$ cells were also cultured in expansion medium composed of HPC expansion medium supplemented with 1% cytokine mix E and 1% penicillin/streptomycin. The cultivation of $CD34^+$ cells on the hydrogels was conducted over a period of 27 days whereby the medium was exchanged twice a week. At the same time, the number of cells was determined and, if necessary, reduced so that the number of cells did not exceed 5×10^5 cells per sample. The total volume was increased to 2 mL after 14 and 17 days, respectively. Half of the volume (1 mL) was replaced by fresh TCD medium on the following day.

Statistical Analysis

Statistical analysis was performed with GraphPad Prism 6 Software. When comparing two means of data, statistical significance was determined by the unpaired two-tailed Student's *t*-test and a set α-level at 0.05.

RESULTS AND DISCUSSION

Nanostructuring and Functionalization of PEG-Based Hydrogels

In order to study the effects of surface-attached Notch ligand DLL1 in different densities on the differentiation of HSPCs to T cells, hydrogels with hexagonally ordered arrays of GNPs in which the nanoparticles are equally spaced over the entire surface area were manufactured. The overall process involved several steps including the deposition of inverse, gold precursor-loaded diblock copolymer micelles on glass substrates via BCML and the subsequent transfer of the reduced GNPs onto the hydrogel (Spatz et al., 2000; Lohmuller et al., 2011). Initially, quasi-hexagonal arrays of GNPs with two different interparticle distances were prepared on glass substrates following an established BCML preparation strategy. The interparticle distances of the GNPs on the glass substrates determines the density of the Notch ligand DLL1 in the manufactured hydrogels. The interparticle distance could be controlled by varying the molecular weight of the applied block copolymer and by varying the fraction ratio between the two blocks. Quasi-hexagonal arrays of GNPs with an average interparticle distance of 42.47 ± 1.41 nm were prepared by employing a block copolymer consisting of 288 styrene subunits and 119 2-vinyl pyridine subunits (PS_{288}-*b*-$P2VP_{119}$, $Đ^* = 1.06$) whereas an average interparticle distance of 90.55 ± 2.23 nm could be reached by employing a block copolymer consisting of 1,056 styrene subunits and 671 2-vinyl pyridine subunits (PS_{1056}-*b*-$P2VP_{671}$, $Đ^* = 1.09$). The two resulting array types will be referred to in the following as GNP-40 and GNP-90. Nanostructured glass substrates were analyzed by SEM in order to assess the interparticle distance as well as the degree of order of the deposited GNPs (**Figure 1A** and **Supplementary Figure 1**). For this purpose, the resulting SEM micrographs were analyzed using a custom-made ImageJ plugin in which a mathematical definition of hexagonallity defined by Williges (Williges et al., 2013) was applied (see section Characterization and Technical Devices). Here, the resulting hexagonal order parameter Ψ_6 is equal to one in case of perfect hexagonal ordering and approaches zero the more random the considered structure becomes. Calculations gave a $\Psi 6$ value of 0.52 ± 0.01 in case of GNP-40 arrays and a Ψ_6 value of 0.54 ± 0.03 for GNP-90 arrays. Both values are acceptable to describe the obtained structures as quasi-hexagonal.

In the following step, the GNPs were transferred from the glass substrates into the PEG-based hydrogels via a copolymerization step. The GNPs had to be equipped with a polymerizable group prior to the polymerization in order to accomplish the transfer. Nanostructured hydrogels applied in this study were synthesized by UV-light induced free-radical copolymerization of PEG-diacrylate with a molecular weight of 700 g/mol (PEG700-DA), RGDSK-PEG-acrylate and *N*,*N*'-bis(acryloyl)-cystamine (BAC). The latter one links the GNPs covalently to the hydrogels during

the reaction. The RGD sequence which was also incorporated in the hydrogels is a minimal cell adhesion motif that is found in many proteins of the extracellular matrix (ECM), for example fibronectin (Klein, 1995). It is commonly used in cell culture applications as it is able to mimic the adhesive properties of the ECM as its structure is recognized by integrin receptors on cell membranes (Winkler et al., 2017). For the purpose of the transfer, the GNPs on the glass substrates were first functionalized with BAC by taking advantage of the strong affinity between elemental gold and thiol groups. Thiolate-gold bonds were formed between BAC and the GNPs during an incubation period upon reduction of BAC to N-(2-mercaptoethyl) acrylamide (Aydin et al., 2010). The surface attached linkers were then available to participate in the free-radical copolymerization of PEG700-DA and RGDSK-PEG-acrylate via their terminal acrylate groups presented on the glass nanoarrays enabling the covalent incorporation of the particles in the hydrogels. Thiolate-gold bonds have strong binding energies between 170 and 200 kJ/mol compared to the relatively weak electrostatic interactions between the GNPs and the glass surfaces. After polymerization and careful detachment of the produced hydrogel from the functionalized glass substrate, the GNPs were successfully transmitted into hydrogels while maintaining their well-defined quasi-hexagonal order as well as their interparticle distances almost completely (Aydin et al., 2010). Experimentally, this was accomplished by employing a custom-made setup which is displayed in **Figure 1B**. The BAC-functionalized glass substrates were placed in a self-made glass mold consisting of microscopy slides and glass cover slips (for technical details see chapter 2.3). The polymerization solution was then pipetted into the resulting gap followed by irradiation with UV-light. In addition, monofunctional unstructured hydrogels consisting only of (PEG700-DA) and RGDSK-PEG-acrylate were synthesized and used as control sample in cell test experiments.

The efficient incorporation of the RGD-sequence in the hydrogel was shown in a previously published study of our group by fluorescence measurements using a FITC-tagged RGD-PEG-acrylate as well as time-of-flight secondary ion mass spectrometry (Winkler et al., 2017). Electroless gold deposition was utilized as indirect verification method to assess the quality of the nanoparticle transfer. The process involved the reduction and subsequent deposition of dissolved gold cations on the surface-attached GNPs in the presence of hydroxylamine as reducing agent, whereby the GNPs act as crystallization nuclei. In doing so, the resulting elemental gold is favored to deposit on the GNPs as this process is thermodynamically preferred as opposed to the formation of new gold particles in solution (Stremsdoerfer et al., 1988; Brown and Natan, 1998; Lohmueller et al., 2008). As a result of the remarkable increase of the GNP size, the color of the hydrogel appeared violet after sufficient immerging time, which is typical for the presence of gold colloids (Everett, 1992). The corresponding glass substrate, on the other hand, remained almost colorless after equal treatment indicating that most of the GNPs were transferred into the hydrogel (**Supplementary Figure 2**). The successful transfer was furthermore verified by SEM analysis of the hydrogel surfaces. **Figure 1C** clearly shows the presence of GNPs on the hydrogel after the transfer process while keeping the quasi-hexagonal order. It is obvious from SEM images, however, that the quality of the quasi-hexagonal order as well as the interparticle distances slightly decreased after the reaction. This effects most likely occurred due to deformation and shrinking of the hydrogels during the drying process prior to SEM analysis. Additional curvature of the hydrogel surface could be caused by the electron beam itself. According to Aydin et al. hydrogels made of PEG700-DA possess a degree of swelling which is equal to 1 when the polymerization solution consists of equal volume fractions of water and PEG (Aydin et al., 2010). We therefore presumed that the degree of order as well as the interparticle distances of GNPs on regularly swollen hydrogels are comparable to those on the corresponding glass substrates. The nanostructured hydrogels were furthermore functionalized with the human Notch ligand DLL1 in order to target the Notch pathway of the applied cells and to induce their differentiation into T cells. The incorporated GNPs served as anchor points for the attachment of the ligand and determined the density of DLL1 in the final product. At first, the thiol-functional linker nitrilotriacetic acid (NTA-thiol) was attached to the GNPs via the formation of a thiol-gold bond. The free carboxylic acid groups of the surface-bound NTA were then used to form a chelate complex with nickel ions. DLL1 was attached in the subsequent step by taking advantage of the strong binding affinity between the nickel complex and the nitrogen atoms of imidazole rings provided by a six-fold histidine sequence (His_6-tag) on the C-terminus of DLL1. This binding strategy via the His_6-Tag to decorate nanostructures with proteins proved also in other studies to be efficient and specific (Aydin et al., 2009; Deeg et al., 2013; Ericsson et al., 2013; Wegner and Spatz, 2013). In this way, the protein could be immobilized in a specific orientation ensuring that the receptor binding side was available for the cells as also shown in previous studies by the Spatz group (Glass et al., 2003; Deeg et al., 2013). Extensive investigations of the binding of DLL1 to gold surfaces in general as well as on to gold nanopatterned hydrogels in particular were shown in a previously published study of our group by QCM-D measurements and immunofluorescent staining using a DLL1 specific antibody, respectively (Winkler et al., 2017). In the current study, homogenous gold surfaces functionalized with DLL1 and the cell adhesive, RGD containing protein fibronectin were prepared and used beside the nanopatterned hydrogels. These samples served as control to investigate the differences in T cell differentiation between DLL1 presented in a defined order and density and DLL1 presented in an unordered manner at higher density.

Adhesion of $CD34^+$ Cells on Nanostructured DLL1-Functionalized Hydrogels

In order to induce the differentiation of primary HSPCs into T cells, $CD34^+$ cells were seeded on DLL1 functionalized hydrogels in the established *in vitro* T cell differentiation system. Initially, the interactions of the cells with the nanostructured bifunctional hydrogels were investigated by SEM to ensure that the cells actually adhered on the RGD containing hydrogels, allowing an interaction between surface immobilized Notch ligand DLL1 and the Notch receptors of the $CD34^+$ cells. **Figure 2** shows

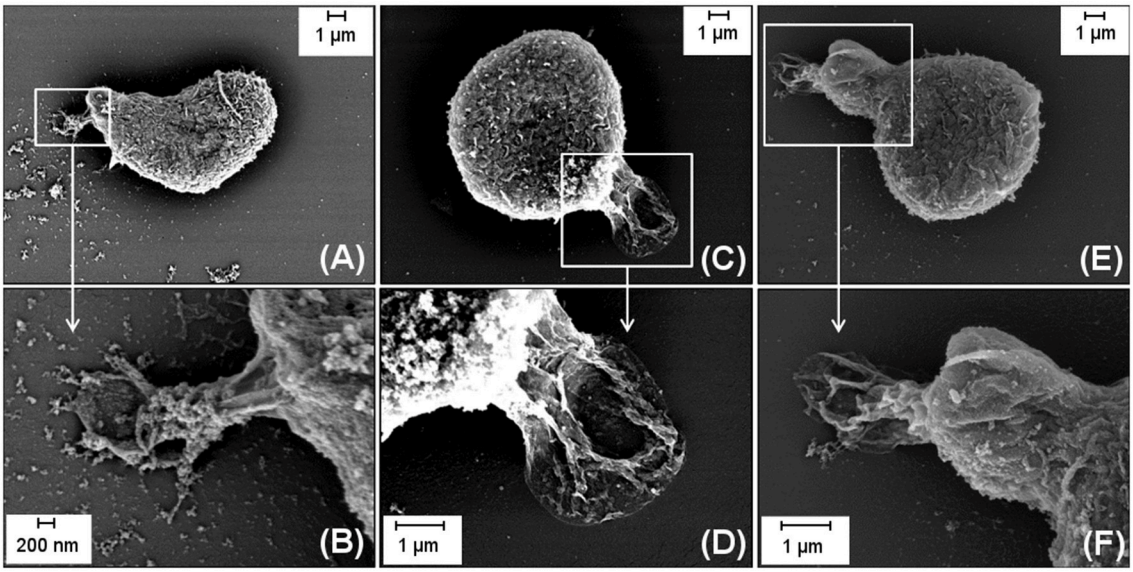

FIGURE 2 | Representative SEM micrographs with different magnifications displaying the adhesive behavior of CD34$^+$ cells seeded on a DLL1/RGD functionalized hydrogel with an average interparticle distance of 40 nm. In the upper row **(A,C,E)** representative images showing one entire cell are depicted. The encircled areas (white rectangles) are magnified in the images displayed in the lower row **(B,D,F)**. **(B)** shows the magnification of the encircled area of **(A)**, **(D)** of **(C)** and **(F)** of **(E)**. Scale bars **(A,C,D,E,F)**: 1 µm; **(B)**: 200 nm.

representative SEM images of CD34$^+$ cells which were incubated on a DLL1 hydrogel with an average interparticle distance of 40 nm. The cells were seeded onto the hydrogel directly after CD34$^+$ isolation. In order to provide sufficient time for cell adhesion, cell culture was conducted overnight in the corresponding expansion medium for CD34$^+$ cells. The images clearly show the formation of cellular protrusions which are in contact with the surface, proving the adhesion of the cells to the bifunctional hydrogel. Furthermore, it could be shown that the adhered cells retained their physiological spherical morphology and, therefore, the bifunctional hydrogel can be considered adhesive for the applied cell type.

Proliferation of CD34$^+$ Cells on Nanostructured DLL1-Functionalized Hydrogels

Human UCB-derived CD34$^+$ cells were cultured for 27 days either on DLL1-nanostructured RGD-hydrogels with an interparticle spacing of ∼40 and 90 nm, respectively, compared with non-structured no-ligand RGD-hydrogel controls, or cultured on gold substrates biofunctionalized with DLL1 and fibronectin. Whereas, the latter culture substrate presents the DLL1 in a randomly ordered distribution in high density as incubated with 5 µg DLL1 ml^{-1}, the gold nanoparticle bound-DLL1 is exposed in a quasi-hexagonal fashion with lower densities, ∼722 molecules DLL1 µm^{-2} for 40 nm interparticle spacing and 141 molecules DLL1 µm^{-2} for the 90 nm interparticle spacing (calculated via the Lagrange densest circle packing as described in Winkler et al. (2017). During the long-term culture of CD34$^+$ cells, cell expansion was examined by counting cells twice a week. The total number of cells continuously increased over the course of 27 days on all investigated surfaces (**Figure 3**) indicating ongoing proliferation. The proliferation promoting effect of our hydrogel system with and without Notch-ligand in comparison to the DLL1-fibronectin-gold and tissue culture plastic (TCP) became first visible after 14 days of culture (**Figure 3**). On day 24/25 the total cell count of the 90 nm DLL1-functionalized RGD-hydrogel culture was significantly elevated compared to the DLL1-fibronectin-gold surface as well as standard culture substrate TCP. This difference regarding TCP surface kept significant also after 27 days of culture (**Figure 3**). At any analyzed time point, no clear difference in total cell number was evident between cells cultured on the DLL1-nanostructured hydrogels with interligand distances of ∼40 and 90 nm and it was also not strikingly different from pure RGD-hydrogel. Hence, the overall proliferation capacity of the total cell population originating from HSPCs was not reduced by induction of Notch signaling by DLL1 at the densities provided by the nanostructured hydrogels. On the basis of a successful protocol for extrathymic human T cell differentiation *in vitro* we used a serum-free medium supplemented with a defined cytokine cocktail as recommended in Pawelec et al. (1998), including additional IL-7 as it has been shown to enhance early T cell differentiation (Ohishi et al., 2002; Varnum-Finney et al., 2003; Ikawa et al., 2010). The absence of serum is a prerequisite for manufacturing of T cells and chemically defined serum replacements are meanwhile as efficient as human or fetal bovine serum for T cell expansion (Smith et al., 2015). Serum-free medium is suggested to provide an even better T cell proliferation environment as recently reported by Xu et al. (2018). We initially tested the total

cell expansion of an identical donor derived $CD34^+$ starting population on TCP in the presence of either HPC expansion medium or TCD medium. Cultures in HPC expansion medium reached ∼10-fold higher cell numbers than cultures in TCD medium after 21 culture days (**Supplementary Figure 3**). Use of the TCD medium for differentiation analysis on the different surfaces resulted in the expansion of the entire cell population to a maximum factor of 39 after 27 days on the pure RGD hydrogel that is ∼2.4-fold higher than TCP (**Figure 3**). The total cell expansion efficiency of HSPCs after 27 days in TCD medium on our bifunctional hydrogel system (32-fold on 40 nm and 30-fold on 90 nm DLL1-RGD-hydrogel) was far below efficiencies reached in a feeder cell-based system in which, e.g., the total cell number of UCB-derived HSPC in OP9-DLL1 coculture increased more than 10,000-fold after a comparable time period of around 4 weeks (Smedt et al., 2011). However, in stromal cell coculture conditions the exact cytokine composition (excreted by the supporting feeder cell layer) is largely undefined and not stable over time. Thus, such not fully defined systems are not suitable for clinical settings.

T Cell Differentiation of $CD34^+$ Cells on Nanostructured DLL1-Functionalized Hydrogels

At day 27, we determined if patterned surface-immobilized DLL1 on RGD hydrogels is capable of directing T lineage differentiation and generating early or late T lymphocytes. Therefore, cultures were analyzed for the presence of CD7 as an early T cell surface marker, as well as CD2, CD3, TCRα/β, CD4, CD8, CD4, CD8 which define sequentially later stages of T cell development (Awong et al., 2009; Meek et al., 2010; Fernandez et al., 2014; Famili et al., 2017). Additional information regarding the various marker molecules are listed in the supporting information (**Supplementary Table 1**). By day 27, the majority of cells from all surface conditions were $CD34^-$ as the frequency of $CD34^+$ cells decreased from a starting population of more than 99% down to <10% of the total population (**Figure 4A**) indicating progressive differentiation. Additionally, we could exclude differentiation toward the B cell lineage as the number of $CD19^+$ cells was very low on all investigated surfaces, and even significantly lower on 90 nm-DLL1-RGD-hydrogels in comparison to the RGD-hydrogel control (**Figure 4B**). Although detectable after 27 days culture, neither $CD7^+$, nor $CD2^+$ cell frequencies were affected by the presentation of immobilized DLL1 (**Figures 4C**,**D**). Later maturational stages of the T cell development are characterized by the sequential expression of $CD4^+$ and $CD8^+$ as double positive ($CD4^+CD8^+$) cells and high levels of CD3 and TCRα/β, that are absolutely necessary for proceeding development into fully mature single positive $CD4^+CD8^-$ or $CD4^-CD8^+$ T cells (Famili et al., 2017). The frequencies of $CD4^+CD8^+$, $CD3^+$, $TCR\alpha/\beta^+$, and $CD3^+TCR\alpha/\beta^+$ cells at day 27 were found to be very low (**Figures 5A–D**,**F**) and the results concerning the expression of these markers by cells in Notch-induced (DLL1) cultures did not differ from no-ligand controls. Of the investigated antigens, only CD4 showed a clear expression (mean > 5% among all surfaces; **Figure 5E**). An upcoming level of $CD4^+$ on the cell surface is in humans characteristic for an intermediate single positive stage (ISP), before developing into double positive $CD4^+CD8^+$ cells, and ultimately into mature single positive $CD4^+$ (Halkias et al., 2014). CD4 is also expressed by monocytes/macrophages and NK cells (Kazazi et al., 1989; Filion et al., 1990; Milush et al., 2009). However, the combination of lymphoid cytokines in the TCD medium with Notch activation via DLL1, which promotes lymphoid differentiation toward T cells (Varnum-Finney et al., 2003; Dallas et al., 2007; Fernandez et al., 2014), makes the induction of myeloid differentiation highly unlikely. As we cannot exactly assign the maturational stage of these generated $CD4^+$ cells, which are at the same time largely $CD3^-$ and $TCR\alpha/\beta^-$, we state that the obtained cells represent a population that has passed an atypical T cell differentiation which is slightly more pronounced on 90 nm DLL1-RGD-hydrogels compared to 40 nm DLL1- or even pure RGD-hydrogels (**Supplementary Figure 4**). However, the 90 nm DLL1-RGD-hydrogel (with 141 molecules DLL μm^{-2}) showed the most promising results in terms of T cell differentiation from UCB-derived HSPCs in combination with the serum-free and cytokine defined TCD medium in comparison to the 40 nm DLL1-hydrogels (722 molecules DLL1 μm^{-2}) and the even more densely packed DLL1-fibronectin gold substrates. Thus, it seems that for T cell differentiation, stimulation by rather low DLL1 surface densities is favorable.

The impact of Notch on T cell differentiation is highly dependent on the respective T cell subpopulation one is looking for. In other studies which also utilized non-cell membrane immobilized DLL1 for T cell differentiation they applied higher densities to a maximum of 10 $\mu g\ ml^{-1}$ for 28 days of HSC culture. Analyzed cell populations were also characterized by the absence of mature T cell marker such as $CD3^+$ (Dallas et al., 2007) or $CD4^+$, $CD8^+$, $CD19^+$ (Varnum-Finney et al., 2003). They generated a substantial amount of early T cells that were defined by $CD25^+$ and $CD44^+CD25^+$ phenotypes, respectively, that are predominantly characteristic for the murine species but different from the phenotype representing human T lineage commitment (Halkias et al., 2014).

To study human T cell differentiation from HSPCs, UCB is an easily available HSPC source that was also used in our experimental design. Several studies investigated the effect of DLL1 on the differentiation of UCB-derived HSPCs. All these studies have in common to predominantly promote early stages of T cell differentiation. Delaney et al. (2005) reported a density-dependent effect of $DLL1^{ext-IgG}$ on the growth and differentiation of hematopoietic cells. They demonstrated an increase in the absolute number of $CD7^+$ cells at $DLL1^{ext-IgG}$ ligand concentrations ranging from 1.25 to 20 $\mu g\ ml^{-1}$ and a progressive increase in the proportion of $CD34^-CD7^+$ cells with increasing concentrations of $DLL1^{ext-IgG}$. In their experiments they used a defined serum-free medium, whereas Fernandez et al. (2014) successfully generated $CD1a^+CD7^+$ and $CD4^+CD8^+$ early T cells in OP9-DLL1 conditioned medium supplemented with human recombinant Flt3L and IL-7 (5 $ng\ ml^{-1}$) on Fc-DLL1 (2.5 $\mu g\ ml^{-1}$) coated plates after 25 days. Ohishi et al. reported that the addition of IL-7 (100 $ng\ ml^{-1}$) to a defined serum-free medium promoted the generation of $CD34^-CD7^+$ cells and

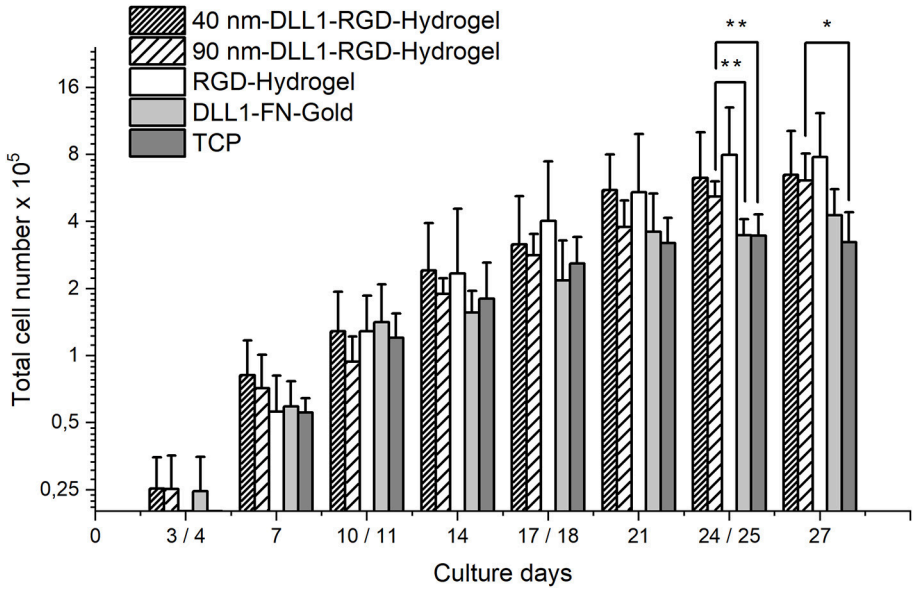

FIGURE 3 | Total number of cells cultured on bifunctional surfaces for 27 days. Cells were generated from 2×10^4 human UCB $CD34^+$ cells on DLL1-nanostructured and pure RGD-PEGDA hydrogels as well as DLL1-non-structured fibronectin (FN) gold substrates. Nanostructures define a DLL1 spacing of 40 and 90 nm, respectively. Viable cells were enumerated at the indicated time points. Standard culture surface is (TCP). Data represent mean (SD) cell numbers from $N = 6$ samples from each surface type, executed in three independent experiments. Significant differences are indicated as follows: $^*P < 0.05$; $^{**}P < 0.01$.

$CD25^+CD7^+$ cells from $CD34^+CD38^+$ UCB-derived HSPCs cultured for 3 weeks in the presence of immobilized $DLL1^{ext-myc}$ (1 μg ml^{-1}) (Ohishi et al., 2002). Notably, no cells expressing surface CD3, TCRαβ, or TCRγδ, or CD19 were detected, an observation that concurs with the very low frequencies of same markers we used in our flow cytometer analysis. The above mentioned effects of the combination of Notch ligand DLL1 and IL-7 to enhance T cell differentiation is also to be seen in a dose dependent manner as OP9-DLL1 cocultures with adult murine hematopoietic progenitors revealed that only low doses (<5 ng ml^{-1}) of IL-7 increased the frequency of $CD4^+CD8^+$ T cells (Huang et al., 2005) and a differentiation from double negative to double positive $CD4^+CD8^+$ T cells is still Notch-dependent but no longer IL-7-dependent (Balciunaite et al., 2005). Similar effects were shown for human HSPCs upon deprivation of IL-7 in OP9-DLL1 cocultures, however only when followed by anti-CD3 stimulation (Patel et al., 2012).

Beside an immediately controllable variation of concentrations of soluble factors such as Flt3L or IL-7 the adjustment of the amount of spatially fixed ligands in an artificial thymic culture system is especially challenging because tethered ligands represent a static environment, while T cell development is a highly dynamic process. During maturation in the thymus, T lymphocytes are migrating through different thymic regions that provide stage-specific developmental signals (Petrie and Zúñiga-Pflücker, 2007). On their way they are sensing different Notch ligands (DLL1, DLL4, JAG1, and JAG2) whose expression is spatially regulated and defines distinct thymic Notch signaling niches (García-León et al., 2018). The main site of T cell maturation is the thymus cortex (Griffith et al., 2009). Analysis of the Notch ligand expression pattern in the human post natal thymus visualized that DLL1 was expressed in both cortical and medullary thymic epithelial cells, whereas most cortical thymic epithelial cells lack DLL4 that is in contrast to mouse (García-León et al., 2018). For mice it turned out that DLL4 is indispensable for T cell commitment and maturation (Hozumi et al., 2008; Koch et al., 2008; Mohtashami et al., 2010) and mouse TCRαβ development requires continuous Notch signaling (Schmitt et al., 2004). By contrast, human TCRαβ development is dependent on the reduction of Notch activation (Van De Walle et al., 2009). Complementary, a Notch1 signaling strength hierarchy among the different Notch ligands has been proposed, with JAG1 being the weakest activator, followed by JAG2, DLL1, and DLL4 as the strongest (Van De Walle et al., 2011). Furthermore, the human Notch1 receptor has shown to be intrinsically selective for DLL4 over DLL1 (Andrawes et al., 2013). Reimann et al. (2012) utilized this strong Notch activation potential and cultured UCB-derived $CD34^+$ cells on immobilized DLL4-Fc (5 μg ml^{-1}) whose progeny showed increasing CD7 expression after day 7 that was correlated with a decrease in CD34 expression. Recently, Shukla et al. (2017) were able to set a concentration threshold >7.5 μg ml^{-1} of plate immobilized DLL4 –Fc that supported early T cell (DN3) cell generation from mouse HSPCs in serum-free medium after 7 d of culture. They further demonstrated with human $CD34^+$ HSPCs derived from UCB that only the combination of DLL4 and VCAM-1 enabled increased expansion of $CD7^+CD34^-$ early T cells in comparison with DLL4 alone or DLL4 with fibronectin or retronectin. This result pointed out that beside the choice of ligand the combination of ligands is determinative to

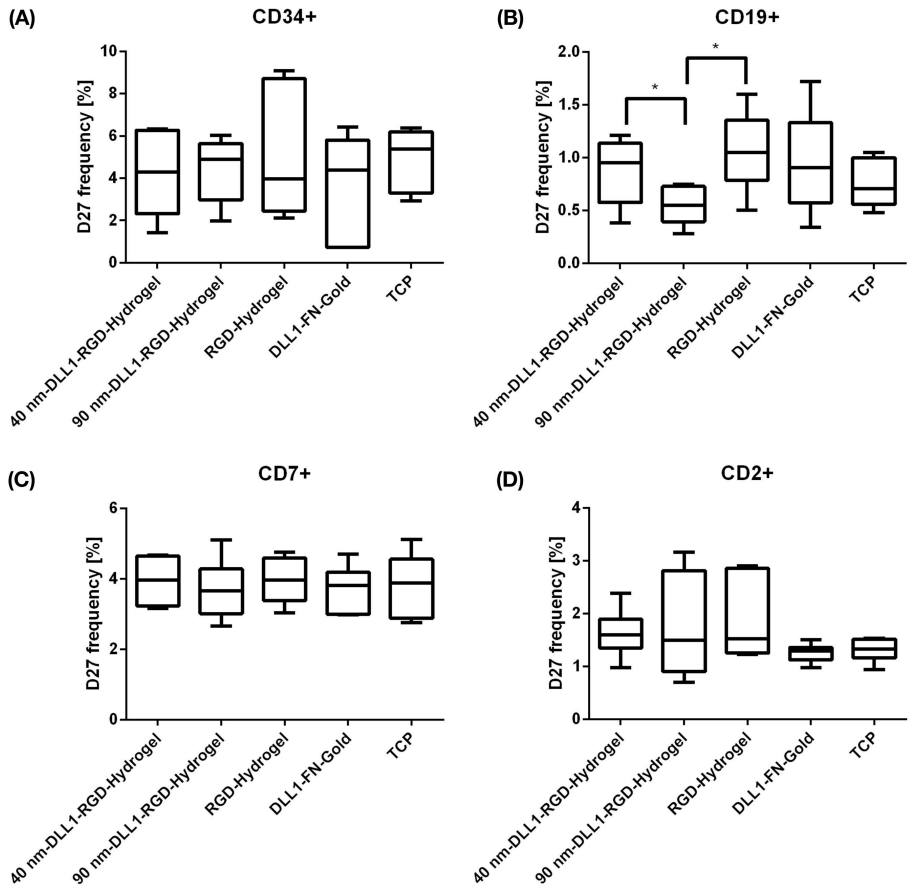

FIGURE 4 | Expression of cell surface markers indicating the stage of T cell differentiation from human UCB CD34$^+$ cells. CD34$^+$ cells were exposed to DLL1-nanostructured and pure RGD-PEGDA hydrogels as well as DLL1-non-structured fibronectin gold substrates in culture of 27 days. DLL1 nanopattern defines an intermolecular spacing of ∼40 and 90 nm, respectively. Cultured cells were analyzed by flow cytometry for surface expression of stem cell marker CD34 **(A)**, B cell marker CD19 **(B)**, CD7 as early T cell marker **(C)** and for a later maturational stage CD2 **(D)**. Data represent percentage of marker positive cells as box plots from $N = 6$ wells of identical surface types from three independent experiments. TCP, tissue culture plastic; FN, fibronectin. Significant differences are indicated $^*P < 0.05$.

elicit synergistic effects for T cell commitment and maturation. Since most Notch ligand-presenting stromal cells are of epithelial nature in the thymus and therefore non-motile, it seems that dynamic changes in the spatial availability of different Notch ligands is tightly connected with the migratory behavior of the T cells, among others regulated by differential expression of integrins and modulation of integrin activation (Mojcik et al., 1995; Savino et al., 2004). The ECM protein fibronectin mediates firm cell adhesion as well as migration via α4β1 and α5β1 integrins in thymocytes shown *in vitro* with late T cells (CD3$^+$CD69$^+$) (Crisa et al., 1996). Fibronectin is expressed predominantly in the thymus medulla (Salomon et al., 1997), whereas the cell surface ligand VCAM-1 is expressed by cortical stromal cells in the thymus, also bound by α4β1 integrin and affecting the adhesion and migration of early T cells (Prockop et al., 2002). Collectively, our bifunctional hydrogels are combining Notch ligand DLL1 and the adhesive RGD-sequence that is, among other integrins, bound by α5β1 (Humphries et al., 2006). Therefore, CD34$^+$ cells exposed to our bifunctional hydrogels were subjected to the cooperative effect of a DLL1-induced Notch signaling and RGD-induced integrin signaling. Thus, we artificially mimicked a thymic Notch signaling niche located to the thymus medulla, where mature single positive T cells are found. The atypical T cell differentiation we demonstrated by the elevated fraction of single positive CD4$^+$ T cells observed on 90 nm DLL1-RGD-hydrogel underpin the represented medullar-like condition.

CONCLUSIONS

In the current study, we tested a bifunctional PEG-based hydrogel containing the cell adhesion supporting motif RGD as well as the human Notch ligand DLL1 for its potential as instructive platform for HSPC differentiation. The gold nanoparticle bound DLL1 is presented in a quasi-hexagonal manner with densities of ∼722 molecules DLL1 μm^{-2} at interparticle distances of ∼40 nm and ∼141 molecules DLL1 μm^{-2} at interparticle distances of ∼90 nm, respectively. For

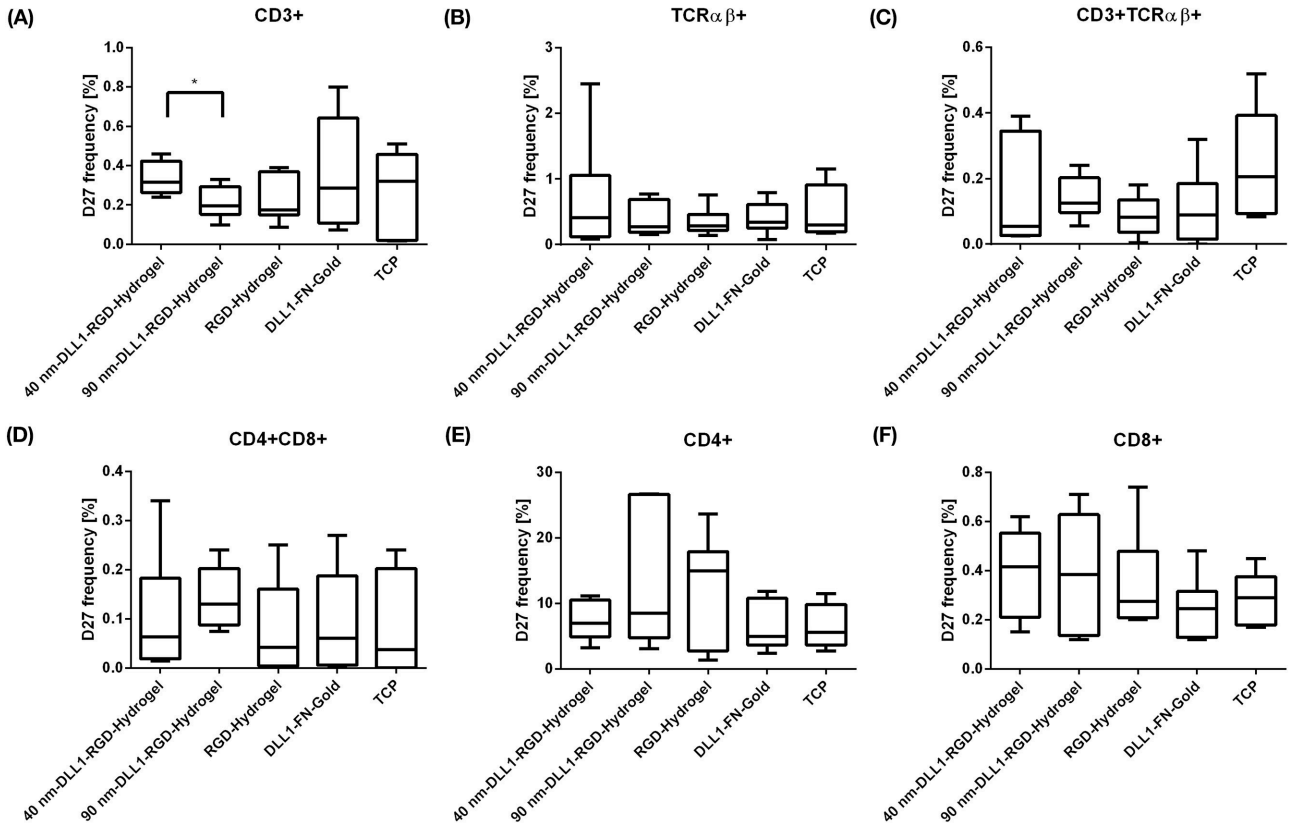

FIGURE 5 | Expression of cell surface markers indicating the stage of T cell differentiation from human UCB CD34$^+$ cells. CD34$^+$ cells were exposed to DLL1-nanostructured and pure RGD-PEGDA hydrogels as well as DLL1-non-structured fibronectin gold substrates in culture of 27 days. DLL1 nanopattern with interparticle spacings of ∼40 and 90 nm were applied. Cultured cells were analyzed by flow cytometry for surface expression of late T cell markers CD3, TCRαβ, CD4, and CD8 as single positive **(A,B,E,F)** or double positive population **(C,D)**. Data presented as box plots showing the percentage of cells positive for the different markers. Data from $N = 6$ samples of each surface type from three independent experiments are shown. TCP, tissue culture plastic; FN, fibronectin. Significant differences are indicated by $^*P < 0.05$.

the first time we applied the described biomaterials for the differentiation of HSPCs to T cells. *In vitro* differentiated T cells are extremely interesting for biomedical applications as they possess a strong potential to reduce side effects and complications arising from HSC transplantations. UCB HSPCs were cultured for 27 days on the different hydrogels as well as reference samples in order to assess their influence on the proliferation and differentiation behavior of the applied cells. Growing in defined serum-free conditions, the total number of cells continuously increased during the culture period on all tested surfaces. Beside the proliferation promoting effect CD 4 was the only examined T cell marker which was expressed in a relevant amount in all samples. Based on these findings, we propose an atypical T lineage differentiation after 27 days in culture. Immobilization of RGD and DLL1 on bifunctionalized hydrogels addressed two important signaling pathways (integrins and Notch) for T cell differentiation, and were combined with effects arisen from soluble components of the utilized cytokine defined T cell differentiation medium. Although the T lineage output was not significantly affected by the quantitative differences in nanopatterned DLL1 presentation, our *in vitro* system induced at least in parts T cell commitment shown by a slightly elevated single positive CD4 T cell fraction and number of obtained CD4$^+$ cells. Thus, it appears that the applied biomaterials artificially mimicked a medullar-like thymic Notch signaling environment. The herein presented culture platform allows for the precise adjustment of tethered ligand densities. However, our data clearly show that controlling the spatial arrangement of the applied ligands is not sufficient for efficiently directing *in vitro* T cell differentiation. *In vivo,* T cell development is dependent on the synergy of multiple molecules, whose expression in the thymus is tightly controlled not only in space but also in time. Thus, our study highlights the need for spatio-temporally adjustable biomaterials in order to achieve bioinstructive platforms for *in vitro* T cell differentiation. In other words, to potentiate the effect of ligand surface distribution, the system needs to implement the dynamic changes in ligand-receptor interaction as it occurs physiologically during T cell development. Then it might contribute to the development of feeder cell-free human T cell differentiation systems that are

indispensable for future clinical applications of *in vitro* generated T cells.

AUTHOR CONTRIBUTIONS

DK and AL-H analyzed the results and wrote the manuscript with contributions from all authors. KJ conducted the experiments and analyzed the results. UG conducted the SEM measurements. CL-T conceived the initial idea, supervised the study, analyzed the results, and did the proofreading of the final manuscript.

FUNDING

The project was funded by the BMBF NanoMatFutur programme (FKZ 13N12968). CL-T and AL-H acknowledge funding by the BioInterfaces in Technology and Medicine programme of the Helmholtz Association. The publication of this article was funded by the Open Access Fund of the Leibniz Universität Hannover.

ACKNOWLEDGMENTS

The authors thank Dr. Toufik Naolou (KIT, Leibniz University Hannover) for illustration of the figure displaying the production of the nanopatterned hydrogels. Furthermore, we are indebted to Anna-Lena Winkler for assistance in execution of the project and Saskia Kraus (KIT) for excellent technical assistance.

SUPPLEMENTARY MATERIAL

The Supplementary Material for this article can be found online at: https://www.frontiersin.org/articles/10.3389/fmats.2018.00081/full#supplementary-material

REFERENCES

Altrock, E., Muth, C. A., Klein, G., Spatz, J. P., and Lee-Thedieck, C. (2012). The significance of integrin ligand nanopatterning on lipid raft clustering in hematopoietic stem cells. *Biomaterials* 33, 3107–3118. doi: 10.1016/j.biomaterials.2012.01.002

Anasetti, C., Aversa, F., and Brunstein, C. G. (2012). Back to the future: mismatched unrelated donor, haploidentical related donor, or unrelated umbilical cord blood transplantation? *Biol. Blood Marrow Transplant.* 18, S161–S165. doi: 10.1016/j.bbmt.2011.11.004

Andrawes, M. B., Xu, X., Liu, H., Ficarro, S. B., Marto, J. A., Aster, J. C., et al. (2013). Intrinsic selectivity of NOTCH 1 for delta-like 4 over delta-like 1. *J. Biol. Chem.* 288, 25477–25489. doi: 10.1074/jbc.M113.454850

Awong, G., Herer, E., Surh, C. D., Dick, J. E., La Motte-Mohs, R. N., and Zúñiga-Pflücker, J. C. (2009). Characterization *in vitro* and engraftment potential *in vivo* of human progenitor t cells generated from hematopoietic stem cells. *Blood* 114, 972–982. doi: 10.1182/blood-2008-10-187013

Aydin, D., Louban, I., Perschmann, N., Blummel, J., Lohmuller, T., Cavalcanti-Adam, E. A., et al. (2010). Polymeric substrates with tunable elasticity and nanoscopically controlled biomolecule presentation. *Langmuir* 26, 15472–15480. doi: 10.1021/la103065x

Aydin, D., Schwieder, M., Louban, I., Knoppe, S., Ulmer, J., Haas, T. L., et al. (2009). Micro-nanostructured protein arrays: a tool for geometrically controlled ligand presentation. *Small* 5, 1014–1018. doi: 10.1002/smll.200801219

Bae, H., Ahari, A. F., Shin, H., Nichol, J. W., Hutson, C. B., Masaeli, M., et al. (2011). Cell-laden microengineered pullulan methacrylate hydrogels promote cell proliferation and 3D cluster formation. *Soft Matter* 7, 1903–1911. doi: 10.1039/C0sm00697A

Bahceci, E., Epperson, D., Douek, D. C., Melenhorst, J. J., Childs, R. C., and Barrett, A. J. (2003). Early reconstitution of the T-cell repertoire after non-myeloablative peripheral blood stem cell transplantation is from post-thymic T-cell expansion and is unaffected by graft-versus-host disease, or mixed chimaerism. *Br. J. Haematol.* 122, 934–943. doi: 10.1046/j.1365-2141.2003.04522.x

Balciunaite, G., Ceredig, R., Fehling, H.-J., Zúñiga-Pflücker, J.-C., and Rolink, A. G. (2005). The role of NOTCH and IL-7 signaling in early thymocyte proliferation and differentiation. *Eur. J. Immunol.* 35, 1292–1300. doi: 10.1002/eji.200425822

Besseyrias, V., Fiorini, E., Strobl, L. J., Zimber-Strobl, U., Dumortier, A., Koch, U., et al. (2007). Hierarchy of Notch-Delta interactions promoting T cell lineage commitment and maturation. *J. Exp. Med.* 204, 331–343. doi: 10.1084/jem.20061442

Boland, G. J., Vlieger, A. M., Ververs, C., and Gast, G. C. (1992). Evidence for transfer of cellular and humoral immunity to cytomegalovirus from donor to recipient in allogeneic bone marrow transplantation. *Clin. Exp. Immunol.* 88, 506–511. doi: 10.1111/j.1365-2249.1992.tb06479.x

Brown, K. R., and Natan, M. J. (1998). Hydroxylamine seeding of colloidal au nanoparticles in solution and on surfaces. *Langmuir* 14, 726–728. doi: 10.1021/la970982u

Carlens, S., Remberger, M., Aschan, J., and Ringdén, O. (2001). The role of disease stage in the response to donor lymphocyte infusions as treatment for leukemic relapse. *Biol. Blood Marrow Transplant.* 7, 31–38. doi: 10.1053/bbmt.2001.v7.pm11215696

Crisa, L., Cirulli, V., Ellisman, M. H., Ishii, J. K., Elices, M. J., and Salomon, D. R. (1996). Cell adhesion and migration are regulated at distinct stages of thymic T cell development: the roles of fibronectin, VLA4, and VLA5. *J. Exp. Med.* 184, 215–228. doi: 10.1084/jem.184.1.215

Dallas, M. H., Varnum-Finney, B., Delaney, C., Kato, K., and Bernstein, I. D. (2005). Density of the Notch ligand Delta1 determines generation of B and T cell precursors from hematopoietic stem cells. *J. Exp. Med.* 201, 1361–1366. doi: 10.1084/jem.20042450

Dallas, M. H., Varnum-Finney, B., Martin, P. J., and Bernstein, I. D. (2007). Enhanced T-cell reconstitution by hematopoietic progenitors expanded *ex vivo* using the Notch ligand Delta1. *Blood* 109, 3579–3587. doi: 10.1182/blood-2006-08-039842

Deeg, J., Axmann, M., Matic, J., Liapis, A., Depoil, D., Afrose, J., et al. (2013). T cell activation is determined by the number of presented antigens. *Nano Lett.* 13, 5619–5626. doi: 10.1021/nl403266t

Delaney, C., Heimfeld, S., Brashem-Stein, C., Voorhies, H., Manger, R. L., and Bernstein, I. D. (2010). Notch-mediated expansion of human cord blood progenitor cells capable of rapid myeloid reconstitution. *Nat. Med.* 16, 232–236. doi: 10.1038/nm.2080

Delaney, C., Varnum-Finney, B., Aoyama, K., Brashem-Stein, C., and Bernstein, I. D. (2005). Dose-dependent effects of the Notch ligand Delta1 on *ex vivo* differentiation and *in vivo* marrow repopulating ability of cord blood cells. *Blood* 106, 2693–2699. doi: 10.1182/blood-2005-03-1131

Douek, D. C., Vescio, R. A., Betts, M. R., Brenchley, J. M., Hill, B. J., Zhang, L., et al. (2000). Assessment of thymic output in adults after haematopoietic stemcell transplantation and prediction of t-cell reconstitution. *Lancet* 355, 1875–1881. doi: 10.1016/S0140-6736(00)02293-5

Drury, J. L., and Mooney, D. J. (2003). Hydrogels for tissue engineering: scaffold design variables and applications. *Biomaterials* 24, 4337–4351. doi: 10.1016/S0142-9612(03)00340-5

Dumont-Girard, F., Roux, E., Van Lier, R. A., Hale, G., Helg, C., Chapuis, B., et al. (1998). Reconstitution of the t-cell compartment after bone marrow transplantation: restoration of the repertoire by thymic emigrants. *Blood* 92, 4464–4471.

Ericsson, E. M., Enander, K., Bui, L., Lundstrom, I., Konradsson, P., and Liedberg, B. (2013). Site-specific and covalent attachment of his-tagged proteins by chelation assisted photoimmobilization: a strategy for microarraying of protein ligands. *Langmuir* 29, 11687–11694. doi: 10.1021/la4011778

Everett, D. H. (1992). *Grundzuege Der Kolloidwissenschaft*. Berlin; Heidelberg: Springer.

Fairbanks, B. D., Schwartz, M. P., Bowman, C. N., and Anseth, K. S. (2009). Photoinitiated polymerization of peg-diacrylate with lithium phenyl-2,4,6-trimethylbenzoylphosphinate: polymerization rate and cytocompatibility. *Biomaterials* 30, 6702–6707. doi: 10.1016/j.biomaterials.2009.08.055

Famili, F., Wiekmeijer, A.-S., and Staal, F. J. (2017). The development of T cells from stem cells in mice and humans. *Future Sci. OA* 3:FSO186. doi: 10.4155/fsoa-2016-0095

Fernandez, I., Ooi, T. P., and Roy, K. (2014). Generation of functional, antigen-specific CD8+ human T cells from cord blood stem cells using exogenous notch and tetramer-TCR signaling. *Stem Cells* 32, 93–104. doi: 10.1002/stem.1512

Ferrara, J. L. M., Levine, J. E., Reddy, P., and Holler, E. (2009). Graft-versus-host disease. *Lancet* 373, 1550–1561. doi: 10.1016/S0140-6736(09)60237-3

Filion, L. G., Izaguirre, C. A., Garber, G. E., Huebsh, L., and Aye, M. T. (1990). Detection of surface and cytoplasmic CD4 on blood monocytes from normal and HIV-1 infected individuals. *J. Immunol. Methods* 135, 59–69. doi: 10.1016/0022-1759(90)90256-U

García-León, M. J., Fuentes, P., De La Pompa, J. L., and Toribio, M. L. (2018). Dynamic regulation of NOTCH1 activation and notch ligand expression in human thymus development. *Development* 145:dev165597. doi: 10.1242/dev.165597

Glass, R., Moller, M., and Spatz, J. P. (2003). Block copolymer micelle nanolithography. *Nanotechnology* 14, 1153–1160. doi: 10.1088/0957-4484/14/10/314

Griffith, A. V., Fallahi, M., Nakase, H., Gosink, M., Young, B., and Petrie, H. T. (2009). Spatial mapping of thymic stromal microenvironments reveals unique features influencing T lymphoid differentiation. *Immunity* 31, 999–1009. doi: 10.1016/j.immuni.2009.09.024

Grob, J. P., Prentice, H. G., Hoffbrand, A. V., Tate, T., Grundy, J. E., Griffiths, P. D., et al. (1987). Immune donors can protect marrow-transplant recipients from severe cytomegalovirus infections. *Lancet* 329, 774–776. doi: 10.1016/S0140-6736(87)92800-5

Gstraunthaler, G., Lindl, T., and Van Der Valk, J. (2013). A plea to reduce or replace fetal bovine serum in cell culture media. *Cytotechnology* 65, 791–793. doi: 10.1007/s10616-013-9633-8

Halkias, J., Melichar, H. J., Taylor, K. T., and Robey, E. A. (2014). Tracking migration during human T cell development. *Cell. Mol. Life Sci.* 71, 3101–3117. doi: 10.1007/s00018-014-1607-2

Hern, D. L., and Hubbell, J. A. (1998). Incorporation of adhesion peptides into nonadhesive hydrogels useful for tissue resurfacing. *J. Biomed. Mater. Res.* 39, 266–276. doi: 10.1002/(SICI)1097-4636(199802)39:2andlt;266::AID-JBM14andgt;3.0.CO;2-B

Holländer, G., Gill, J., Zuklys, S., Iwanami, N., Liu, C., and Takahama, Y. (2006). Cellular and molecular events during early thymus development. *Immunol. Rev.* 209, 28–46. doi: 10.1111/j.0105-2896.2006.00357.x

Hozumi, K., Mailhos, C., Negishi, N., Hirano, K.-I., Yahata, T., Ando, K., et al. (2008). Delta-like 4 is indispensable in thymic environment specific for T cell development. *J. Exp. Med.* 205, 2507–2513. doi: 10.1084/jem.20080134

Huang, J., Garrett, K. P., Pelayo, R., Zúñiga-Pflücker, J. C., Petrie, H. T., and Kincade, P. W. (2005). Propensity of adult lymphoid progenitors to progress to DN2/3 stage thymocytes with notch receptor ligation. *J Immunol.* 175, 4858–4865. doi: 10.4049/jimmunol.175.8.4858

Humphries, J. D., Byron, A., and Humphries, M. J. (2006). Integrin ligands at a glance. *J. Cell Sci.* 119, 3901–3903. doi: 10.1242/jcs.03098

Ikawa, T., Hirose, S., Masuda, K., Kakugawa, K., Satoh, R., Shibano-Satoh, A., et al. (2010). An essential developmental checkpoint for production of the T cell lineage. *Science* 329, 93–96. doi: 10.1126/science.1188995

Kazazi, F., Mathijs, J.-M., Foley, P., and Cunningham, A. L. (1989). Variations in CD4 expression by human monocytes and macrophages and their relationship to infection with the human immunodeficiency virus. *J. Gen. Virol.* 70, 2661–2672. doi: 10.1099/0022-1317-70-10-2661

Klein, G. (1995). The extracellular-matrix of the hematopoietic microenvironment. *Experientia* 51, 914–926. doi: 10.1007/BF01921741

Koch, U., Fiorini, E., Benedito, R., Besseyrias, V., Schuster-Gossler, K., Pierres, M., et al. (2008). Delta-like 4 is the essential, nonredundant ligand for NOTCH1 during thymic T cell lineage commitment. *J. Exp. Med.* 205, 2515–2523. doi: 10.1084/jem.20080829

Kolb, H., Mittermuller, J., Clemm, C., Holler, E., Ledderose, G., Brehm, G., et al. (1990). Donor leukocyte transfusions for treatment of recurrent chronic myelogenous leukemia in marrow transplant patients. *Blood* 76, 2462–2465.

La Motte-Mohs, R. N., Herer, E., and Zúñiga-Pflücker, J. C. (2005). Induction of T-cell development from human cord blood hematopoietic stem cells by delta-like 1 *in vitro*. *Blood* 105, 1431–1439. doi: 10.1182/blood-2004-04-1293

Lewin, S. R., Heller, G., Zhang, L., Rodrigues, E., Skulsky, E., Van Den Brink, M. R. M., et al. (2002). "Direct evidence for new T-cell generation by patients after either T-cell–depleted or unmodified allogeneic hematopoietic stem cell transplantations" *Presented in part in abstract form at the 42nd Annual Meeting of the American Society of Hematology* (San Francisco, CA), 2235–2242.

Lohmueller, T., Bock, E., and Spatz, J. P. (2008). Synthesis of quasi-hexagonal ordered arrays of metallic nanoparticles with tuneable particle size. *Adv. Mater.* 20, 2297–2302. doi: 10.1002/adma.200702635

Lohmuller, T., Aydin, D., Schwieder, M., Morhard, C., Louban, I., Pacholski, C., et al. (2011). Nanopatterning by block copolymer micelle nanolithography and bioinspired applications. *Biointerphases* 6, MR1–12. doi: 10.1116/1.3536839

Meek, B., Cloosen, S., Borsotti, C., Van Elssen, C. H. M. J., Vanderlocht, J., Schnijderberg, M. C. A., et al. (2010). *In vitro*–differentiated T/natural killer–cell progenitors derived from human CD34+ cells mature in the thymus. *Blood* 115, 261–264. doi: 10.1182/blood-2009-05-223990

Milner, L., Kopan, R., Martin, D., and Bernstein, I. D. (1994). A human homologue of the drosophila developmental gene, Notch, is expressed in $cd34^+$ hematopoietic precursors. *Blood* 83, 2057–2062.

Milush, J. M., Long, B. R., Snyder-Cappione, J. E., Cappione, A. J., York, V. A., Ndhlovu, L. C., et al. (2009). Functionally distinct subsets of human NK cells and monocyte/DC-like cells identified by coexpression of CD56, CD7, and CD4. *Blood* 114, 4823–4831. doi: 10.1182/blood-2009-04-216374

Mohtashami, M., Shah, D. K., Nakase, H., Kianizad, K., Petrie, H. T., and Zúñiga-Pflücker, J. C. (2010). Direct comparison of DLL1- and DLL4-mediated notch activation levels shows differential lymphomyeloid lineage commitment outcomes. *J. Immunol.* 185, 867–876. doi: 10.4049/jimmunol.1000782

Mojcik, C., Salomon, D., Chang, A., and Shevach, E. (1995). Differential expression of integrins on human thymocyte subpopulations. *Blood* 86, 4206–4217.

Moss, P., and Rickinson, A. (2005). Cellular immunotherapy for viral infection after HSC transplantation. *Nature Rev. Immunol.* 5:9. doi: 10.1038/nri1526

Murphy, K. M., Travers, P., and Walport, M., (2002). *Janeway Immunologie*. Berlin; Heidelberg: Springer Spektrum.

Muth, C. A., Steinl, C., Klein, G., and Lee-Thedieck, C. (2013). Regulation of hematopoietic stem cell behavior by the nanostructured presentation of extracellular matrix components. *PLoS ONE* 8:e54778. doi: 10.1371/journal.pone.0054778

Nguyen, K. T., and West, J. L. (2002). Photopolymerizable hydrogels for tissue engineering applications. *Biomaterials* 23, 4307–4314. doi: 10.1016/S0142-9612(02)00175-8

Ogawa, M. (1993). Differentiation and proliferation of hematopoietic stem cells. *Blood* 81, 2844–2853.

Ohishi, K., Varnum-Finney, B., and Bernstein, I. D. (2002). Delta-1 enhances marrow and thymus repopulating ability of human CD34(+) CD38(-) cord blood cells. *J. Clin. Invest.* 110, 1165–1174. doi: 10.1172/JCI0216167

Park, K.-D., Marti, L., Kurtzberg, J., and Szabolcs, P. (2006). *In vitro* priming and expansion of cytomegalovirus- specific Th1 and Tc1 t cells from naive cord blood lymphocytes. *Blood* 108, 1770–1773. doi: 10.1182/blood-2005-10-006536

Patel, E. S., Okada, S., Hachey, K., Yang, L.-J., Durum, S. K., Moreb, J. S., et al. (2012). Regulation of in vitro human t cell development through interleukin-7 deprivation and anti-cd3 stimulation. *BMC Immunol.* 13:46. doi: 10.1186/1471-2172-13-46

Pawelec, G., Muller, R., Rehbein, A., Hahnel, K., and Ziegler, B. L. (1998). Extrathymic t cell differentiation *in vitro* from human CD34+ stem cells. *J. Leukoc. Biol.* 64, 733–739. doi: 10.1002/jlb.64.6.733

Petrie, H. T., and Zúñiga-Pflücker, J. C. (2007). Zoned out: functional mapping of stromal signaling microenvironments in the thymus. *Annu. Rev. Immunol.* 25, 649–679. doi: 10.1146/annurev.immunol.23.021704.115715

Platzman, I., Muth, C. A., Lee-Thedieck, C., Pallarola, D., Atanasova, R., Louban, I., et al. (2013). Surface properties of nanostructured bio-active interfaces: impacts of surface stiffness and topography on cell–surface interactions. *RSC Adv.* 3, 13293–13303. doi: 10.1039/c3ra41579a

Prockop, S. E., Palencia, S., Ryan, C. M., Gordon, K., Gray, D., and Petrie, H. T. (2002). Stromal cells provide the matrix for migration of early

lymphoid progenitors through the thymic cortex. *J. Immunol.* 169, 4354–4361. doi: 10.4049/jimmunol.169.8.4354

Radtke, F., Wilson, A., Stark, G., Bauer, M., Van Meerwijk, J., Macdonald, H. R., et al. (1999). Deficient T cell fate specification in mice with an induced inactivation of NOTCH1. *Immunity* 10, 547–558. doi: 10.1016/S1074-7613(00)80054-0

Reimann, C., Six, E., Dal-Cortivo, L., Schiavo, A., Appourchaux, K., Lagresle-Peyrou, C., et al. (2012). Human T-lymphoid progenitors generated in a feeder-cell-free delta-like-4 culture system promote t-cell reconstitution in NOD/SCID/γc(-/-) mice. *Stem Cells* 30, 1771–1780. doi: 10.1002/stem.1145

Rink, L., Kruse, A., and Haase, H., (2015). *Immunologie Für Einsteiger*. Berlin; Heidelberg: Springer Spektrum

Roux, E., Dumont-Girard, F., Starobinski, M., Siegrist, C.-A., Helg, C., Chapuis, B., et al. (2000). Recovery of immune reactivity after T-cell–depleted bone marrow transplantation depends on thymic activity. *Blood* 96, 2299–2303.

Salomon, D. R., Crisa, L., Mojcik, C. F., Ishii, J. K., Klier, G., and Shevach, E. M. (1997). Vascular cell adhesion molecule-1 is expressed by cortical thymic epithelial cells and mediates thymocyte adhesion. Implications for the function of α4β1 (vla4) integrin in T-cell development. *Blood* 89, 2461–2471.

Savino, W., Mendes-Da-Cruz, D. A., Smaniotto, S., Silva-Monteiro, E., and Villa-Verde, D. M. S. (2004). Molecular mechanisms governing thymocyte migration: combined role of chemokines and extracellular matrix. *J. Leukoc. Biol.* 75, 951–961. doi: 10.1189/jlb.1003455

Schmid, C., Schleuning, M., Schwerdtfeger, R., Hertenstein, B., Mischak-Weissinger, E., Bunjes, D., et al. (2006). Long-term survival in refractory acute myeloid leukemia after sequential treatment with chemotherapy and reduced-intensity conditioning for allogeneic stem cell transplantation. *Blood* 108, 1092–1099. doi: 10.1182/blood-2005-10-4165

Schmitt, T. M., Ciofani, M., Petrie, H. T., and Zúñiga-Pflücker, J. C. (2004). Maintenance of T cell specification and differentiation requires recurrent notch receptor–ligand interactions. *J. Exp. Med.* 200, 469–479. doi: 10.1084/jem.20040394

Schmitt, T. M., and Zúñiga-Pflücker, J. C. (2002). Induction of t cell development from hematopoietic progenitor cells by delta-like-1 *in vitro*. *Immunity* 17, 749–756. doi: 10.1016/S1074-7613(02)00474-0

Schmitt, T. M., and Zúñiga-Pflücker, J. C. (2006). T-cell development, doing it in a dish. *Immunol. Rev.* 209, 95–102. doi: 10.1111/j.0105-2896.2006.00353.x

Schütt, C., and Broeker, B. (2011). *Grundwissen Immunologie*. Heidelberg: Spektrum Akademischer Verlag. doi: 10.1007/978-3-8274-2647-5

Seet, C. S., He, C., Bethune, M. T., Li, S., Chick, B., Gschweng, E. H., et al. (2017). Generation of mature T cells from human hematopoietic stem and progenitor cells in artificial thymic organoids. *Nat. Methods* 14, 521–530. doi: 10.1038/nmeth.4237

Shlomchik, W. D. (2007). Graft-versus-host disease. *Nat. Rev. Immunol.* 7:340. doi: 10.1038/nri2000

Shukla, S., Langley, M. A., Singh, J., Edgar, J. M., Mohtashami, M., Zúñiga-Pflücker, J. C., et al. (2017). Progenitor T-cell differentiation from hematopoietic stem cells using delta-like-4 and VCAM-1. *Nat. Methods* 14:531. doi: 10.1038/nmeth.4258

Smedt, M. D., Hoebeke, I., and Plum, J. (2004). Human bone marrow CD34+ progenitor cells mature to t cells on OP9-DL1 stromal cell line without thymus microenvironment. *Blood Cells Mol. Dis.* 33, 227–232. doi: 10.1016/j.bcmd.2004.08.007

Smedt, M. D., Leclercq, G., Vandekerckhove, B., Kerre, T., Taghon, T., and Plum, J. (2011). T-lymphoid differentiation potential measured *in vitro* is higher in CD34+CD38-/LO hematopoietic stem cells from umbilical cord blood than from bone marrow and is an intrinsic property of the cells. *Haematologica* 96, 646–654. doi: 10.3324/haematol.2010.036343

Smith, C., Økern, G., Rehan, S., Beagley, L., Lee, S. K., Aarvak, T., et al. (2015). *Ex vivo* expansion of human T cells for adoptive immunotherapy using the novel xeno-free cts immune cell serum replacement. *Clin.Transl. Immunol.* 4:e31. doi: 10.1038/cti.2014.31

Spatz, J. P., Mossmer, S., Hartmann, C., Moller, M., Herzog, T., Krieger, M., et al. (2000). Ordered deposition of inorganic clusters from micellar block copolymer films. *Langmuir* 16, 407–415. doi: 10.1021/la990070n

Stremsdoerfer, G., Perrot, H., Martin, J. R., and Clechet, P. (1988). Autocatalytic deposition of gold and palladium onto n-gaas in acidic media. *J. Electrochem. Soc.* 135, 2881–2886. doi: 10.1002/chin.198915344

Van Coppernolle, S., Verstichel, G., Timmermans, F., Velghe, I., Vermijlen, D., Smedt, M. D., et al. (2009). Functionally mature CD4 and CD8 tcralphabeta cells are generated in OP9-DL1 cultures from human CD34+ hematopoietic cells. *J. Immunol.* 183, 4859–4870. doi: 10.4049/jimmunol.0900714

Van De Walle, I., De Smet, G., Gärtner, M., De Smedt, M., Waegemans, E., Vandekerckhove, B., et al. (2011). Jagged2 acts as a delta-like NOTCH ligand during early hematopoietic cell fate decisions. *Blood* 117, 4449–4459. doi: 10.1182/blood-2010-06-290049

Van De Walle, I., Smet, G. D., Smedt, M. D., Vandekerckhove, B., Leclercq, G., Plum, J., et al. (2009). An early decrease in notch activation is required for human TCR-alphabeta lineage differentiation at the expense of TCR-gammadelta T cells. *Blood* 113, 2988–2998. doi: 10.1182/blood-2008-06-164871

Van De Walle, I., Waegemans, E., Medts, J. D., Smet, G. D., Smedt, M. D., Snauwaert, S., et al. (2013). Specific NOTCH receptor-ligand interactions control human TCR-αβ/γδ development by inducing differential NOTCH signal strength. *J. Exp. Med.* 210, 683–697. doi: 10.1084/jem.20121798

Varnum-Finney, B., Brashem-Stein, C., and Bernstein, I. D. (2003). Combined effects of notch signaling and cytokines induce a multiple log increase in precursors with lymphoid and myeloid reconstituting ability. *Blood* 101, 1784–1789. doi: 10.1182/blood-2002-06-1862

Varnum-Finney, B., E Purton, L., Yu, M., Brashem-Stein, C., Flowers, D., Staats, S., et al. (1998). The Notch ligand, jagged-1, influences the development of primitive hematopoietic precursor cells. *Blood* 91, 4084–4091.

Varnum-Finney, B., Xu, L., Brashem-Stein, C., Nourigat, C., Flowers, D., Bakkour, S., et al. (2000). Pluripotent, cytokine-dependent, hematopoietic stem cells are immortalized by constitutive NOTCH1 signaling. *Nat. Med.* 6, 1278–1281. doi: 10.1038/81390

Weber, J. M., and Calvi, L. M. (2010). NOTCH signaling and the bone marrow hematopoietic stem cell niche. *Bone* 46, 281–285. doi: 10.1016/j.bone.2009.08.007

Wegner, S. V., and Spatz, J. P. (2013). Cobalt(III) as a stable and inert mediator ion between NTA and HIS6-tagged proteins. *Angew. Chem. Int. Ed. Engl.* 52, 7593–7596. doi: 10.1002/anie.201210317

Welniak, L. A., Blazar, B. R., and Murphy, W. J. (2007). Immunobiology of allogeneic hematopoietic stem cell transplantation. *Annu. Rev. Immunol.* 25, 139–170. doi: 10.1146/annurev.immunol.25.022106.141606

Williges, C., Chen, W., Morhard, C., Spatz, J. P., and Brunner, R. (2013). Increasing the order parameter of quasi-hexagonal micellar nanostructures by ultrasound annealing. *Langmuir* 29, 989–993. doi: 10.1021/la303991x

Winkler, A.-L., Von Wulffen, J., Rödling, L., Raic, A., Reinartz, I., Schug, A., et al. (2017). Significance of nanopatterned and clustered DLL1 for hematopoietic stem cell proliferation. *Adv. Funct. Mater.* 27:1606495. doi: 10.1002/adfm.201606495

Xu, H., Wang, N., Cao, W., Huang, L., Zhou, J., and Sheng, L. (2018). Influence of various medium environment to *in vitro* human t cell culture. *In vitro Cell. Dev. Biol. Anim.* 54,559–566. doi: 10.1007/s11626-018-0273-3

Zhang, W., Ning, C., Xu, W., Hu, H., Li, M., Zhao, G., et al. (2018a). Precision-guided long-acting analgesia by GEL-immobilized bupivacaine-loaded microsphere. *Theranostics* 8, 3331–3347. doi: 10.7150/thno.25276

Zhang, W., Xu, W., Ning, C., Li, M., Zhao, G., Jiang, W., et al. (2018b). Long-acting hydrogel/microsphere composite sequentially releases dexmedetomidine and bupivacaine for prolonged synergistic analgesia. *Biomaterials* 181, 378–391. doi: 10.1016/j.biomaterials.2018.07.051

Zheng, Y., Cheng, Y., Chen, J., Ding, J., Li, M., Li, C., et al. (2017). Injectable hydrogel–microsphere construct with sequential degradation for locally synergistic chemotherapy. *ACS Appl. Mater. Interface* 9, 3487–3496. doi: 10.1021/acsami.6b15245

Conflict of Interest Statement: The authors declare that the research was conducted in the absence of any commercial or financial relationships that could be construed as a potential conflict of interest.